Mechanics of Materials 126 (2018) 148–162

Contents lists available at ScienceDirect

Mechanics of Materials

journal homepage: www.elsevier.com/locate/mechmat

Validation of recent analytical dilatational models for porous polycrystals using crystal plasticity finite element models with Schmid and non-Schmid activation laws

Daniel J. Savage[a], Nitin Chandola[b], Oana Cazacu[b,*], Brandon A. McWilliams[c], Marko Knezevic[a,*]

[a] Department of Mechanical Engineering, University of New Hampshire, Durham, NH 03824, USA
[b] Department of Mechanical and Aerospace Engineering, University of Florida/REEF, Shalimar, FL 32579, USA
[c] Weapons and Materials Research Directorate, US Army Research Laboratory, Aberdeen Proving Ground, MD 21005, USA

ARTICLE INFO

Keywords:
Voided polycrystals
Crystal plasticity
Non-Schmid effects
Analytic criteria for porous materials
Void evolution
Tension–compression asymmetry

ABSTRACT

Recent analytic criteria for isotropic porous materials developed by Cazacu et al. (2013) revealed the importance of considering specificities of plastic behavior in the matrix. On one hand it was shown that if the matrix material is governed by the von Mises criterion, the yield surface of the porous material should be centrosymmetric and, with the exception of hydrostatic and purely deviatoric loadings, there are combined effects of the mean stress and third-invariant of the stress deviator on void growth or collapse; but on the other hand if the matrix plastic deformation displays strength differential (SD) effects, the response is also sensitive to third-invariant and there is a lack of symmetry of the yield surface of the porous material. In this paper, we use a unit cell modeling approach in conjunction with a crystal plasticity finite element model to verify these theoretical predictions. It is assumed that each porous polycrystal contains a regular array of initially spherical voids and a random initial texture. At the grain-level, we consider that plastic deformation is governed by Schmid law and a recent non-Schmid formulation by Savage et al. (2017a) that intrinsically accounts for tension–compression asymmetry in a physical sense. Unit cell FE calculations are performed for axisymmetric tensile and compressive loadings corresponding to a fixed value of the stress triaxiality and the two possible values of the Lode parameter. The resulting numerical points representing the homogenized yield surfaces and void growth/collapse curves are found to be in agreement with the analytical model's predictions.

1. Introduction

It is well accepted that ductile failure of polycrystalline metallic materials is due to the nucleation, growth, and coalescence of voids (Anderson, 2017; Hosokawa et al., 2012; McClintock, 1968). Void growth is the result of the plastic deformation of the fully-dense material (matrix); therefore, to estimate the rate of void evolution it is imperative to know the plastic potential of the void-matrix aggregate. Based on rigorous limit analysis theorems, Gurson (1977) derived an analytic plastic potential for materials containing randomly distributed spherical voids in a matrix obeying von Mises isotropic yield criterion (i.e., J_2 plasticity). Based on finite-element (FE) unit cell calculations, additional parameters q_1, q_2, q_3 were introduced in Gurson's criterion by Tvergaard (1981). This modified Gurson model, known as Gurson–Tvergaard–Needleman (GTN) model reproduces qualitatively the essential features of tensile fracture of axisymmetric specimens (Tvergaard and Needleman, 1984).

In the past decade, experimental data under a variety of loadings have shown the role played by all stress invariants on failure. In particular, the combined effects of the second and third invariant of the stress deviator (i.e., Lode parameter) have been well documented (Barsoum and Faleskog, 2007; Dunand and Mohr, 2011; Lou and Huh, 2013). Using the full-field dilatational viscoplastic fast Fourier transform (FFT)-based approach of Lebensohn et al. (2011), Lebensohn and Cazacu (2012) performed simulations for both tensile and compressive loadings and showed that yielding of a porous solid with von Mises matrix should involve a very specific coupling between the mean stress and the third-invariant of the stress deviator. However, the effects of this coupling on void growth or collapse were not reported. Using kinematic homogenization and Hill–Mandel lemma (Hill, 1967; Mandel, 1973), (Cazacu et al., 2013) provided an explanation of these combined effects of mean stress and third-invariant on the dilatational response of porous von Mises materials. Furthermore, these authors developed a new analytic plastic potential that captures the aforementioned trends.

* Corresponding authors.
E-mail addresses: cazacu@reef.ufl.edu (O. Cazacu), marko.knezevic@unh.edu (M. Knezevic).

https://doi.org/10.1016/j.mechmat.2018.08.004
Received 4 December 2017; Received in revised form 18 July 2018; Accepted 16 August 2018
Available online 18 August 2018
0167-6636/

Comparison between predictions of the void evolution using this plastic potential and FE cell calculations with a Von Mises matrix reported in Alves et al. (2014) showed good agreement.

In all the aforementioned contributions on porous solids, the plastic deformation of the matrix (i.e., void-free material) is considered to be plastically incompressible. FE unit cell model calculations and analytical criteria for porous solids with plastically compressible matrices have also been proposed. For example, in the case when the matrix obeys Drucker–Prager mean-stress-dependent criterion, FE calculations of yielding of the porous solid were reported by Trillat et al. (2006) while analytical criteria were developed by Barthélémy and Dormieux (2004) and Guo et al. (2008). It is to be noted that in all these models the strength-differential (SD) effects or tension–compression asymmetry in the mechanical response of the respective porous solids are due to the dependence of the matrix plastic behavior on mean stress.

For certain fully-dense polycrystalline metallic materials SD effects are observed even though plastic deformation does not depend on the mean stress (e.g., for body-centered cubic (BCC) metals (Alleman et al., 2014; Knezevic et al., 2015a; Patra et al., 2014; Zecevic et al., 2016b), for hexagonal close-packed (HCP) metals (Gilles et al., 2011; Knezevic et al., 2013a; Knezevic et al., 2010; Knezevic et al., 2015b; Nixon et al., 2010; Zecevic et al., 2017; Zecevic et al., 2018), for orthorhombic metals (Knezevic et al., 2012; Knezevic et al., 2016a; Knezevic et al., 2013b; Zecevic et al., 2016a)). Pressure independent SD effects have been explained by single-crystal plastic deformation mechanisms. For example, in their theoretical study Hosford and Allen (1973) demonstrated that if the plastic deformation is accommodated only by crystallographic twinning, the yield stress in uniaxial tension of a randomly oriented face-centered cubic (FCC) polycrystal should be about 25% lower than that in uniaxial compression and the effect is reversed (i.e., 25% higher in uniaxial compression) for body-centered cubic (BCC) polycrystals. If an FCC material deforms by crystallographic slip and twinning, the difference between the uniaxial yield stresses in tension and compression is smaller but of the same sign (for more details, see Hosford and Caddell (1993)). Also, if the plastic deformation by crystallographic slip does not obey the classical Schmid law, a polycrystalline material may display a slight tension–compression asymmetry (see results on columnar ice reported by Lebensohn et al. (2009)); simulations for polycrystalline molybdenum reported by Gröger et al. (2008) and Savage et al. (2017a)).

Cazacu et al. (2006) proposed a yield criterion for fully-dense, incompressible polycrystalline materials that display SD effects. This criterion involves a unique parameter k, which is expressible in terms of the ratio of the uniaxial yield stresses in tension and compression. Using a kinematic limit-analysis approach, Cazacu and Stewart (2009) developed an analytic plastic potential for isotropic porous solids with a matrix governed by the (Cazacu et al., 2006) yield criterion. The (Cazacu and Stewart 2009) analytic criterion involves all stress invariants and the porosity. Model parameters are related to the plastic properties of the matrix and depend on k. Using (Cazacu and Stewart, 2009) criterion, it was demonstrated that even a very small difference between the uniaxial yield in tension and compression of the matrix has a dramatic influence on yielding of the porous material. Later, by performing an FE investigation on the damage of notched rounded tensile specimens, Cazacu et al. (2013) showed that the rate of void growth and the damage distribution are significantly affected by the tension/compression asymmetry ratio of the matrix. The highest rate of void growth is for materials characterized by $k > 0$ and the lowest rate of void growth corresponds to materials characterized by $k < 0$. Recently, Alves and Cazacu (Alves et al., 2014; Revil-Baudard et al., 2016) conducted three-dimensional (3D) FE unit cell calculations for porous solids with matrix governed by the isotropic form of the (Cazacu et al., 2006) yield criterion. Calculations were performed for materials with matrix characterized by $k > 0$ (uniaxial yield in tension larger than the uniaxial yield in compression), materials with matrix characterized by $k = 0$ (von Mises), and materials with matrix characterized by $k < 0$ (uniaxial yield in compression larger than the uniaxial yield in tension). For each porous material, the imposed macroscopic loadings were such that the principal values of the macroscopic stresses, $\Sigma_1, \Sigma_2, \Sigma_3$ followed a prescribed proportional loading history. It was shown that the stress path history has a very strong effect on the plasticity-damage couplings. For loadings at positive third-stress invariant, ($J_3^{\Sigma} > 0$), the rate of void growth is the slowest for the material characterized by $k < 0$, but the critical zone in the deformation process (onset of coalescence to failure) is very limited. However, for equibiaxial tension loadings, which corresponds to negative third-stress invariant ($J_3^{\Sigma} < 0$) comparison between the rate of void growth and ductility in the same materials lead to completely different findings: the materials characterized by $k < 0$ have the lowest ductility.

A number of studies have been conducted using the unit cell modeling approach pioneered by Gurson (1977) and Koplik and Needleman (1988) to analyze void evolution in a single crystal matrix. Among the studies on the dilatational response of single crystals using three-dimensional (3D) unit cell models (Srivastava and Needleman, 2015; Srivastava et al., 2017a; Yerra et al. 2010) have shown that the effects of J_3^{Σ} (or the Lode parameter) on void evolution are strongly dependent on the crystal orientation.

In this paper, we use the unit cell modeling approach in conjunction with crystal plasticity finite element (CPFE) model to study the dilatational response of porous polycrystals and evaluate the very specific effects of the plastic deformation of the matrix on yielding and void evolution that were put into evidence by recent analytic criteria. Section 2 briefly summarizes these analytic criteria. The CPFE unit cell modeling approach is presented in Section 3. Simulations are conducted for porous BCC polycrystals for which at the grain-level the plastic deformation is governed by Schmid law and a recent formulation of that accounts for tension–compression asymmetry (Savage et al., 2017a). It is assumed that each porous polycrystal contains a regular array of initially spherical voids and a random initial texture. The unit cell FE calculations are performed for axisymmetric tensile and compressive loadings corresponding to a fixed value of the stress triaxiality and the two possible values of the Lode parameter. Special attention is given to ensure the stress triaxiality is constant during the 3D-FE cell model simulations. To impose the boundary conditions a new procedure through a user element (UEL) subroutine is developed in ABAQUS. Results are presented in Section 4. For validation purposes, the numerical yield points obtained with the CPFE unit cell are compared to numerical unit cell results obtained using J_2 plasticity model for the matrix, and the theoretical yield surfaces according to Cazacu et al. (2013). Void growth/collapse for axisymmetric loadings are simulated and found to be in agreement with the calculations obtained using J_2 based FE cell calculations and with the theoretical predictions.

Furthermore, in polycrystals for which the single-crystal plastic deformation mechanisms are responsible for SD effects (the non-Schmid law), the dilatational response is compared to the predictions of the (Cazacu and Stewart, 2009) model. A summary of the main findings and conclusions are presented in Section 5.

Regarding notations, vector and tensors are denoted by boldface characters. If $\mathbf{A}$ is a second-order tensor, $\mathbf{A}^T$ denotes its transpose, i.e. $A_{ij}^T = A_{ji}$ with $i, j = 1,\ldots,3$, tr$\mathbf{A}$ denotes its trace, while det$\mathbf{A}$ denotes its determinant; the contracted product between two symmetric tensors $\mathbf{A}$, and $\mathbf{B}$, is defined as: $\mathbf{A}\cdot\mathbf{B} = \mathrm{tr}(\mathbf{A}\mathbf{B}^T)$; the dyadic product of any two vectors, $\mathbf{a}$ and $\mathbf{b}$ is a second-rank tensor defined as: $\mathbf{a} \otimes \mathbf{b} = a_i b_j$. Scalars and tensor components are denoted as italic and not bold.

2. Analytic isotropic plastic potentials for porous solids

This section summarizes the analytical yield criteria for voided polycrystals used in this work.

2.1. Cazacu et al. (2013) model for porous solids with von Mises matrix

The (Gurson, 1977) plastic potential is expressed as:

$$\Phi(\Sigma_m, \Sigma_e, f) = \left(\frac{\Sigma_e}{\sigma_T}\right)^2 + 2f\cosh\left(\frac{3\Sigma_m}{2\sigma_T}\right) - 1 - f^2 = 0 \tag{1}$$

In the above equation, f is the porosity volume fraction, $\Sigma_e = \sqrt{\frac{3}{2}\text{tr}(\boldsymbol{\Sigma}'^2)}$ is the von Mises effective stress, $\Sigma_m = \text{tr}(\boldsymbol{\Sigma})/3$ is the mean stress, σ_T is the uniaxial tensile yield stress of the matrix (void-free material), and $\boldsymbol{\Sigma}'$ is the deviator of the stress $\boldsymbol{\Sigma}$. If $f = 0$, Eq. (1) reduces to the von Mises yield criterion. It is also worth noting that according to Gurson's criterion there is no effect of the sign of the mean stress on yielding of a porous Mises material:

$$\Phi(\Sigma_m, \Sigma_e, f) = \Phi(-\Sigma_m, \Sigma_e, f). \tag{2}$$

Recently, it was demonstrated that these strong symmetry properties of the yield locus are a direct consequence of Gurson's approximation of the local plastic dissipation (Cazacu et al., 2013). Furthermore, the authors conducted a limit-analysis study and derived a new analytic criterion for a porous von Mises material. According to this criterion: (i) yielding depends on the sign of , the third-invariant of $\boldsymbol{\Sigma}'$; (ii) for stress triaxialities $T = \Sigma_m/\Sigma_e$ different from 0 and $\pm\infty$, there exists a very specific coupling between J_3^Σ and Σ_m. Specifically, the yield point characterized by $J_3^\Sigma \geq 0$ and a given stress-triaxiality T is symmetric, with respect to the axis $\Sigma_m = 0$, to the yield point characterized by $J_3^\Sigma \leq 0$ and $(-T)$.

The parametric representation of this criterion for the different axisymmetric loading cases is:

a) For $J_3^\Sigma \leq 0$, $\Sigma_m \geq 0$, and any value of u:

$$\begin{cases} \frac{\Sigma_m}{\sigma_T} = \frac{1}{9}\frac{1-f}{u} + \frac{1}{3}\ln\left(\frac{u^2-uf+f^2}{u^2-u+1}\frac{1}{f^2}\right) \\ \quad + \frac{1}{18\sqrt{3}}\ln\left(\frac{u+\sqrt{3uf}+f}{u-\sqrt{3uf}+f}\right)\left(\frac{9u^2+3uf+f^2}{u^{3/2}\sqrt{f}}\right) \\ \quad - \frac{1}{18\sqrt{3}}\ln\left(\frac{u+\sqrt{3u}+1}{u-\sqrt{3u}+1}\right)\left(\frac{9u^2+3u+1}{u^{3/2}}\right) \\ \quad + \frac{2}{18\sqrt{3}}\left(\tan^{-1}\left(2\sqrt{\frac{u}{f}}+\sqrt{3}\right) - \tan^{-1}\left(2\sqrt{\frac{u}{f}}-\sqrt{3}\right)\right) \\ \quad - \frac{2}{18\sqrt{3}}(\tan^{-1}(2\sqrt{u}+\sqrt{3}) - \tan^{-1}(2\sqrt{u}-\sqrt{3})) \\ \frac{\Sigma_e}{\sigma_T} = \frac{1-f}{2} + \frac{1}{4\sqrt{3u}}\left[(u^2-u+1)\ln\left(\frac{u+\sqrt{3u}+1}{u-\sqrt{3u}+1}\right)\right. \\ \quad \left. - \frac{(u^2-uf+f^2)}{\sqrt{f}}\ln\left(\frac{u+\sqrt{3uf}+f}{u-\sqrt{3uf}+f}\right)\right] \end{cases} \tag{3}$$

b) For $J_3^\Sigma \leq 0$ and $\Sigma_m \leq 0$:

(b_1) If$u \leq f$:

$$\begin{cases} \frac{\Sigma_m}{\sigma_T} = \frac{f-1}{9u} + \frac{1}{3}\ln\left(\frac{u^2+uf+f^2}{(u^2+1+u)f^2}\right) - \frac{1}{9\sqrt{3fu^3}}\left((9u^2-3uf+f^2)\tan^{-1}\left(\frac{\sqrt{3uf}}{f-u}\right)\right. \\ \quad \left. - (9u^2-3u+1)\tan^{-1}\left(\frac{\sqrt{3u}}{1-u}\right)\right) \\ \quad - \frac{2}{9\sqrt{3}}\left(\tan^{-1}\left(\frac{2\sqrt{u}+\sqrt{f}}{\sqrt{3f}}\right) + \tan^{-1}\left(\frac{2\sqrt{u}-1}{\sqrt{3}}\right)\right. \\ \quad \left. - \tan^{-1}\left(\frac{2\sqrt{u}-\sqrt{f}}{\sqrt{3f}}\right) - \tan^{-1}\left(\frac{2\sqrt{u}+1}{\sqrt{3}}\right)\right) \\ \frac{\Sigma_e}{\sigma_T} = \frac{f|u-1|-|u-f|}{2u} - \frac{1}{2\sqrt{3}}\left[\frac{(u^2+uf+f^2)\tan^{-1}\left(\frac{\sqrt{3uf}}{|f-u|}\right)}{\sqrt{uf}} - \frac{(1+u+u^2)\tan^{-1}\left(\frac{\sqrt{3u}}{|1-u|}\right)}{\sqrt{u}}\right] \end{cases} \tag{4}$$

(b_2) If$f < u < 1$:

$$\begin{cases} \frac{\Sigma_m}{\sigma_T} = \frac{2}{3}\ln(3) - \frac{2}{18}\frac{\pi}{\sqrt{3}} - \frac{1+f-2u}{9u} - \frac{1}{3}\ln\left(\frac{(u^2+1+u)(u^2+uf+f^2)}{f^2}\right) \\ \quad + \frac{1}{9\sqrt{3u^3}}\left((9u^2-3u+1)\arctan\left(\frac{\sqrt{3u}}{1-u}\right)\right. \\ \quad \left. - (9u^2-3uf+f^2)\arctan\left(\frac{\sqrt{3fu}}{f-u}\right)\right) \\ \quad + \frac{2}{9\sqrt{3}}\left(\arctan\left(\frac{2\sqrt{u}+\sqrt{f}}{\sqrt{3f}}\right) - \arctan\left(\frac{2\sqrt{u}-\sqrt{f}}{\sqrt{3f}}\right) + \arctan\left(\frac{2\sqrt{u}+1}{\sqrt{3}}\right)\right. \\ \quad \left. - \arctan\left(\frac{2\sqrt{u}-1}{\sqrt{3}}\right)\right) \\ \frac{\Sigma_e}{\sigma_T} = \frac{1}{2}(1+f) - u + \frac{1}{2\sqrt{3u}}\left(\frac{(u^2+uf+f^2)}{\sqrt{f}}\tan^{-1}\left(\frac{\sqrt{3uf}}{f-u}\right)\right. \\ \quad \left. + (u^2+1+u)\tan^{-1}\left(\frac{\sqrt{3u}}{1-u}\right)\right) \end{cases} \tag{5}$$

(b_3) If$u \geq 1$:

$$\begin{cases} \frac{\Sigma_m}{\sigma_T} = \frac{1-f}{9u} - \frac{1}{3}\ln\left(\frac{u^2+uf+f^2}{(u^2+1+u)f^2}\right) + \frac{1}{9\sqrt{3fu^3}}\left((9u^2-3uf+f^2)\tan^{-1}\left(\frac{\sqrt{3uf}}{f-u}\right)\right. \\ \quad \left. - (9u^2-3u+1)\tan^{-1}\left(\frac{\sqrt{3u}}{1-u}\right)\right) \\ \quad + \frac{2}{9\sqrt{3}}\left(\tan^{-1}\left(\frac{2\sqrt{u}+\sqrt{f}}{\sqrt{3f}}\right) + \tan^{-1}\left(\frac{2\sqrt{u}-1}{\sqrt{3}}\right)\right. \\ \quad \left. - \tan^{-1}\left(\frac{2\sqrt{u}-\sqrt{f}}{\sqrt{3f}}\right) - \tan^{-1}\left(\frac{2\sqrt{u}+1}{\sqrt{3}}\right)\right) \\ \frac{\Sigma_e}{\sigma_T} = \frac{f|u-1|-|u-f|}{2u} - \frac{1}{2\sqrt{3}}\left[\frac{(u^2+uf+f^2)\tan^{-1}\left(\frac{\sqrt{3uf}}{|f-u|}\right)}{\sqrt{uf}} - \frac{(1+u+u^2)\tan^{-1}\left(\frac{\sqrt{3u}}{|1-u|}\right)}{\sqrt{u}}\right] \end{cases} \tag{6}$$

a) For $J_3^\Sigma \geq 0$ and $\Sigma_m \geq 0$:

$$\begin{cases} \frac{\Sigma_m}{\sigma_T} = -\frac{\Sigma_m}{\sigma_T}|_{J_3^\Sigma \leq 0, \Sigma_m \leq 0} \\ \frac{\Sigma_e}{\sigma_T} = \frac{\Sigma_e}{\sigma_T}|_{J_3^\Sigma \leq 0, \Sigma_m \leq 0} \end{cases}, \tag{7}$$

the right-hand expressions being given by Eqs. ((4)-((6)).

b) For $J_3^\Sigma \geq 0$ and $\Sigma_m \leq 0$:

$$\begin{cases} \frac{\Sigma_m}{\sigma_T} = -\frac{\Sigma_m}{\sigma_T}|_{J_3^\Sigma \leq 0, \Sigma_m \geq 0} \\ \frac{\Sigma_e}{\sigma_T} = \frac{\Sigma_e}{\sigma_T}|_{J_3^\Sigma \leq 0, \Sigma_m \geq 0} \end{cases} \tag{8}$$

where the right-hand expressions are given by Eq. (3) (for details on the derivations, see Cazacu et al. (2013)).

In the above expressions, the parameter u is the strain-rate triaxiality defined as $u = \frac{2|D_m|}{D_e}$, where $D_m = \frac{1}{3}\text{tr}\mathbf{D}$ and $D_e = \sqrt{\frac{2}{3}\text{tr}(\mathbf{D}'^2)}$ denote the first and second-invariant of the rate of stretching tensor $\mathbf{D}$, respectively.

As an example, the projection of the yield surface for the porous solid is shown in Fig. 1 according to (Cazacu et al., 2013) criterion Eqs. (3)–((8)) corresponding to $J_3^\Sigma \geq 0$ and $J_3^\Sigma \leq 0$, respectively, and the Gurson yield surface Eq. (1)) for a porosity $f = 0.05$. For purely deviatoric loading (triaxiality $T = 0$), the response is the same while for all other finite triaxialities T the response is softer for $J_3^\Sigma \geq 0$ than for $J_3^\Sigma \leq 0$. For triaxialities approaching infinity, the effect of J_3^Σ starts to decrease, and the yield surfaces for $J_3^\Sigma \geq 0$ and for $J_3^\Sigma \leq 0$ coincide at the

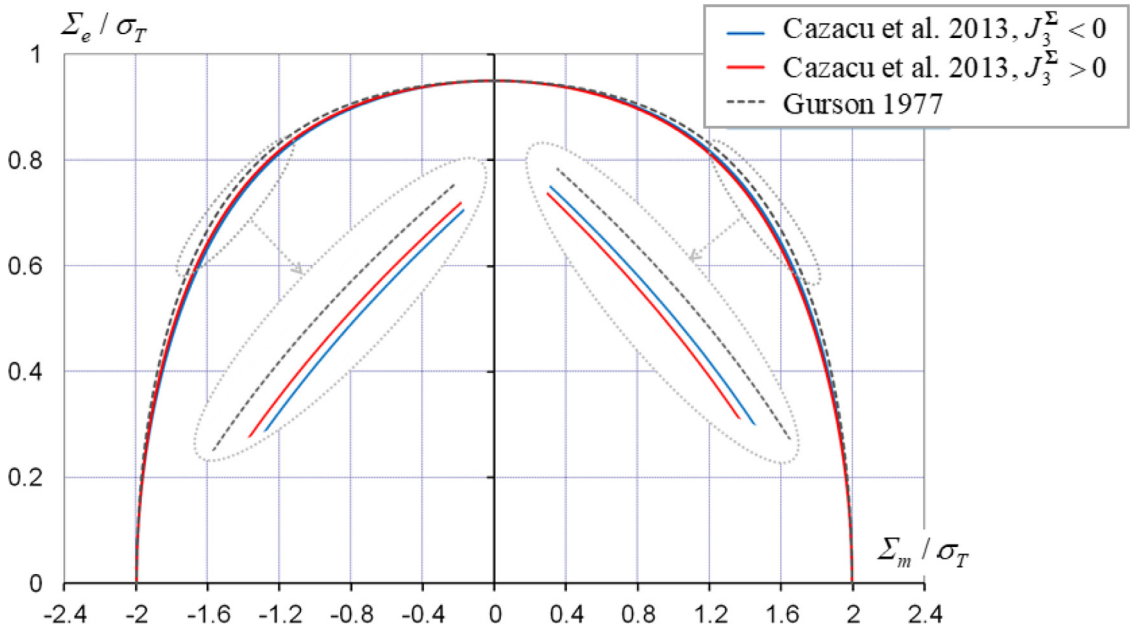

Fig. 1. Yield surface of the porous solid according to Cazacu et al. (2013) criterion for axisymmetric stress states for loadings such that $J_3^{\Sigma} \leq 0$ and $J_3^{\Sigma} \geq 0$, respectively, in comparison with Gurson's (1977) for the same porosity ($f = 0.05$).

purely hydrostatic point. It is clearly seen that Gurson's criterion (Eq. (1)) is an upper-bound of Cazacu et al. (2013) criterion (Eqs. (3)–(8)).

2.2. *Cazacu and Stewart (2009) yield criterion for porous materials*

Cazacu and Stewart (2009) developed an isotropic plastic potential for porous solids containing randomly distributed spherical voids expressed as:

$$\phi(\boldsymbol{\Sigma}, f) = \frac{9}{2(3k^2 - 2k + 3)} \sum_{i=1}^{3} \left(\frac{|\Sigma'_i| - k\Sigma'_i}{\sigma_T} \right)^2 + 2f \cosh\left(z_s \frac{3\Sigma_m}{2\sigma_T} \right) - (1 + f^2) \tag{9}$$

where Σ'_1, Σ'_2, Σ'_3 are the principal values of the deviator of the Cauchy stress tensor $\boldsymbol{\Sigma}'$, f is the void volume fraction, and k is a material parameter associated with plastic tension–compression asymmetry effects in the matrix. It is worth noting that since the criterion (Eq. 9) was derived using rigorous upscaling methods using for the description of the plastic behavior of the matrix (Cazacu et al., 2006) yield criterion; its dependence on the mean stress, Σ_m, was deduced and not postulated. Consequently, the parameter z_s has a clear physical significance, being dependent on the specificities of the plastic deformation, through k, and of the state of stress. Its expression is:

$$z_s = \begin{cases} 1 & \text{if } \Sigma_m \leq 0 \\ \sqrt{\frac{3k^2 + 2k + 3}{3k^2 - 2k + 3}} & \text{if } \Sigma_m > 0 \end{cases} \tag{10}$$

For a fully-dense material, i.e. $f = 0$, $\phi(\boldsymbol{\Sigma}, f)$ given by Eq. (9) reduces to the yield function of the matrix, i.e. the isotropic quadratic form of the (Cazacu et al., 2006) criterion:

$$\frac{9}{2(3k^2 - 2k + 3)} [(|\Sigma'_1| - k\Sigma'_1)^2 + (|\Sigma'_2| - k\Sigma'_2)^2 + (|\Sigma'_3| - k\Sigma'_3)^2] = \sigma_T \tag{11}$$

The rate of change of the void volume fraction, $\dot{f}$, is considered to result only from the growth of existing voids. Thus, the void evolution is obtained from mass conservation and the use of the associated plastic flow rule in conjunction with Eq. (9) as:

$$\mathbf{D}^p \cdot \mathbf{I} = \dot{\lambda} \mathrm{tr}\left(\frac{\partial \phi(\boldsymbol{\Sigma}, f)}{\partial \boldsymbol{\Sigma}} \right) = \dot{\lambda} z_s \frac{f}{\sigma_T} \sinh\left(\frac{3}{2} z_s \frac{\Sigma_m}{\sigma_T} \right), \tag{12}$$

where $\dot{\lambda}$ stands for the plastic multiplier rate. Note that the void evolution depends on the parameter k (see also Eq. (10) for the expression of z_s) and the imposed stress and strain.

As already mentioned, the dilatational response according to (Cazacu and Stewart, 2009) criterion has been compared to FE cell calculation results (Cazacu and Stewart, 2009) or to numerical yield points obtained using full-field dilatational viscoplastic Fast Fourier Transform (FFT) approach (Lebensohn and Cazacu, 2012; Lebensohn et al., 2011). In this paper, the features of the dilatational response of porous materials revealed by Cazacu et al. (2013) for a porous Mises material and by Cazacu and Stewart (2009) for isotropic porous materials with matrix displaying SD effects are verified on the basis of FE cell calculations results for porous isotropic BCC polycrystals. The polycrystal model used in the FE calculations and the unit cell method of analysis are presented in the next section.

3. Crystal plasticity finite element (CPFE) unit cell model

This section reminds of the standard crystal plasticity model formulation and describes the numerical simulation setup developed in this work for dilatational plasticity simulations.

3.1. *Crystal plasticity model*

The kinematics of crystal plasticity follows (Ardeljan et al., 2017; Ardeljan et al., 2016; Ardeljan et al., 2015; Kalidindi et al., 1992), where it is assumed that the total deformation gradient tensor $\mathbf{F}$ can be decomposed as:

$$\mathbf{F} = \mathbf{F}^* \mathbf{F}^p, \tag{13}$$

where $\mathbf{F}^*$ accounts for both elastic stretching as well as lattice rotation, while $\mathbf{F}^p$ denotes the deformation gradient due to plastic deformation alone. $\mathbf{F}^*$ is further employed to define the Green–Lagrange strain,

$$\mathbf{E}^* = \frac{1}{2} \left\{ \mathbf{F}^{\left(*^T\right)} \mathbf{F}^* - \mathbf{I} \right\}. \tag{14}$$

Hooke's law is used to describe elastic behavior, so the second-order Piola–Kirchoff stress in the crystal,

$$\mathbf{T}^* = \mathbf{F}^{\left(*^{(-1)}\right)}\{(\det\mathbf{F}^*)\sigma\}\mathbf{F}^{\left(*^{(-T)}\right)}, \tag{15}$$

is related to $\mathbf{E}^*$ as

$$\mathbf{T}^* = \mathbf{C}\mathbf{E}^*, \tag{16}$$

where $\mathbf{C}$ is the fourth-order elasticity tensor. Plastic deformation is only accommodated by crystallographic slip and for cubic crystals, it is generally assumed that crystallographic slip obeys classical Schmid law. Therefore, slip system, α, is operational if the resolved shear stress

$$\tau^\alpha = \mathbf{P}^\alpha_{sc}\cdot\mathbf{T}^*, \tag{17}$$

surpasses the slip resistance threshold τ^α_c. The Schmid tensor is formed per slip system as the product between the slip normal $\mathbf{n}^\alpha_0$ and slip direction $\mathbf{b}^\alpha_0$ in the initial configuration

$$\mathbf{P}^\alpha_{sc} = \frac{1}{2}(\mathbf{b}^\alpha_0 \otimes \mathbf{n}^\alpha_0 + \mathbf{n}^\alpha_0 \otimes \mathbf{b}^\alpha_0). \tag{18}$$

To predict observed SD effects in BCC materials, we will also consider a non-Schmid law of the type first proposed by Dao and Asaro (1993), Ghorbanpour et al. (2017), Knezevic et al. (2014) and Savage et al. (2017a) that considers that slip initiation depends on both the normal and shear stress acting on the slip plane,

$$\tau^\alpha = \mathbf{P}^\alpha_{sc}\cdot\mathbf{T}^* + \mathbf{P}^\alpha_{ns}\cdot\mathbf{T}^* = \mathbf{P}^\alpha_{tot}\cdot\mathbf{T}^* \tag{19}$$

where

$$\begin{aligned}\mathbf{P}^\alpha_{ns} \;=\; & c_1(\mathbf{t}^\alpha_0 \otimes \mathbf{b}^\alpha_0) + c_2(\mathbf{t}^\alpha_0 \otimes \mathbf{n}^\alpha_0) + c_3(\mathbf{n}^\alpha_0 \otimes \mathbf{n}^\alpha_0) + c_4(\mathbf{t}^\alpha_0 \otimes \mathbf{t}^\alpha_0) \\ & -(c_3 + c_4)(\mathbf{b}^\alpha_0 \otimes \mathbf{b}^\alpha_0),\end{aligned} \tag{20}$$

and the total Schmid tensor $\mathbf{P}^\alpha_{tot}$ is a weighted sum of Schmid and non-Schmid stresses on the slip plane. Recently in Savage et al. (2017a) it was shown that the two shear stresses $\mathbf{t}\otimes\mathbf{b}$ and $\mathbf{t}\otimes\mathbf{n}$ acting normal to the Burgers vector did not have a significant effect on the yield surface for random textured polycrystals, while the normal stresses $\mathbf{n}\otimes\mathbf{n}$, $\mathbf{t}\otimes\mathbf{t}$, and $\mathbf{b}\otimes\mathbf{b}$ significantly affected dislocation motion, producing strong SD effects in random textured polycrystals. To remove pressure dependence in the slip criterion, $\mathbf{b}\otimes\mathbf{b}$ is weighted as a combination of c_3 and c_4 as discussed in Lim et al. (2013) and implemented in Eq. (20).

Irrespective of the criterion for activation for crystallographic slip, the plastic velocity gradient, $\mathbf{L}^p = \dot{\mathbf{F}}^p(\mathbf{F}^p)^{-1}$ can be written as:

$$\mathbf{L}^p = \sum_\alpha \dot\gamma_\alpha(\mathbf{b}^\alpha_0 \otimes \mathbf{n}^\alpha_0), \tag{21}$$

where $\dot\gamma_\alpha$ is the plastic shear strain rate of the system α, and $\mathbf{b}^\alpha_0$ and $\mathbf{n}^\alpha_0$ denote the slip direction and the slip plane normal of the slip systems, respectively, in the initial unloaded configuration. To calculate the plastic shear strain rates $\dot\gamma_\alpha$, the following power-law relationship (Asaro and Needleman, 1985) is employed:

$$\dot\gamma^\alpha = \dot\gamma^\alpha_0\left(\frac{|\tau^\alpha|}{\tau^\alpha_c}\right)^n \mathrm{sgn}(\tau^\alpha_c). \tag{22}$$

In Eq. (22), $\dot\gamma^\alpha_0$ denotes a reference value of the slip rate (taken here as 0.001 s^{-1}) and n represents the strain rate sensitivity exponent taken here as 50, making Eq. (22) nearly rate insensitive. The choice of n is of particular importance in the calculation of gauge yield surfaces of the polycrystal and will be discussed in Section 4 (Knezevic et al., 2016b; Lebensohn et al., 2012; Savage et al., 2017b). In the present study, minimal hardening of the slip resistances is considered to ensure that the overall plastic behavior of the polycrystal is approximately perfectly plastic. The spin of the crystal trihedron, which is used to approximate the lattice spin, is given by Lipinski and Berveiller (1989) and Peeters et al. (2001):

$$\mathbf{W}^* = \mathbf{W}^{app} - \mathbf{W}^p,\ \mathbf{W}^p = \frac{1}{2}(\mathbf{L}^p - \mathbf{L}^{pT}), \tag{23}$$

where $\mathbf{W}^{app}$ is the applied overall spin on the polycrystal and $\mathbf{W}^p$ is the plastic spin (skew-symmetric component of $\mathbf{L}^p$ defined in Eq. (21)).

In this work, we consider only BCC polycrystals in which Schmid and non-Schmid stresses are applied to $\{1\bar10\}\langle111\rangle$ and $\{11\bar2\}\langle111\rangle$ slip modes. These two slip modes are most often studied experimentally and used for modeling partly because slip on {123} planes can be expressed as a combination of slip on {110} and {112} planes (Franciosi, 1983 and Franciosi, 1985) and because texture and stress–strain modeling show good agreement with both slip modes (Alleman et al., 2014; Ardeljan et al., 2014; Ito and Vitek, 2001; Knezevic et al., 2014; Ma et al., 2007; Savage et al., 2017a; Wang and Beyerlein, 2011). Due to the generic nature of this study, we assume that both slip modes have the same starting slip resistance, τ_c, for all slip systems.

3.2. Unit cell model

It is assumed that the porous polycrystal contains a regular array of initially spherical voids. The inter-void spacing is considered to be the same in any direction, and thus the unit cell is initially cubic with side lengths $2C_0$ and contains a single void of radius r_0 at its center. The initial porosity is:

$$f_0 = \frac{\pi}{6}\left(\frac{r_0}{C_0}\right)^3. \tag{24}$$

One-eighth of the FE mesh of the unit cell is shown in Fig. 2. Cartesian tensor notation is used and the center of the coordinate frame is placed at the center of the initially spherical void. The edges of the unit cell are parallel to the axes and the main loading direction is parallel to the 2-axis. Calculations were performed for an initial porosity $f_0 = 0.0104$. In the FE mesh, each element is considered to be a grain with a single starting orientation. The size of the elements and the grains are in this manner linked. A mesh sensitivity study was performed to ensure results became independent on the mesh in terms of both the numerical method and the effective grain size. The results reported hereafter were obtained with structured meshes of 12,871 ABAQUS C3D8 (continuum 3D eight-nodal) elements with selective reduced integration to mitigate volume locking effects. Each mesh was further refined around the void to ensure mesh quality during void growth/collapse (see Fig. 2b). Because every element has eight integration points, the FE unit cells considered for the two initial porosities contained 102,968 and 99,128 crystal orientations, respectively.

The macroscopic stress state imposed on the unit cell is such that the principal values of the macroscopic Cauchy stresses, Σ_1, Σ_2, Σ_3, follow an axisymmetric stress path, i.e. $\Sigma_1 = \Sigma_3$, and a loading history such that the stress triaxiality, T, is constant. Note that for the loading path considered, the mean stress is

$$\Sigma_m = (2\Sigma_1 + \Sigma_2)/3, \tag{25}$$

and the von Mises equivalent stress is:

$$\Sigma_{eq} = |\Sigma_1 - \Sigma_2|. \tag{26}$$

Thus, the stress-triaxiality is

$$T = (2\Sigma_1 + \Sigma_2/|\Sigma_1 - \Sigma_2|), \tag{27}$$

and the third invariant of the stress deviator becomes:

$$J^\Sigma_3 = \Sigma'_1\Sigma'_2\Sigma'_3 = \frac{-2}{27}(\Sigma_1 - \Sigma_2)^3. \tag{28}$$

To study the effect of the third-invariant J^Σ_3 on the behavior of the voided polycrystal, we will investigate loadings corresponding to either the axial stress larger than the lateral stress or vice-versa (i.e., loadings at $J^\Sigma_3 > 0$ and loadings corresponding to $J^\Sigma_3 < 0$, respectively).

To impose the boundary conditions and ensure a constant stress triaxiality T on the unit cell during the entire loading history, an

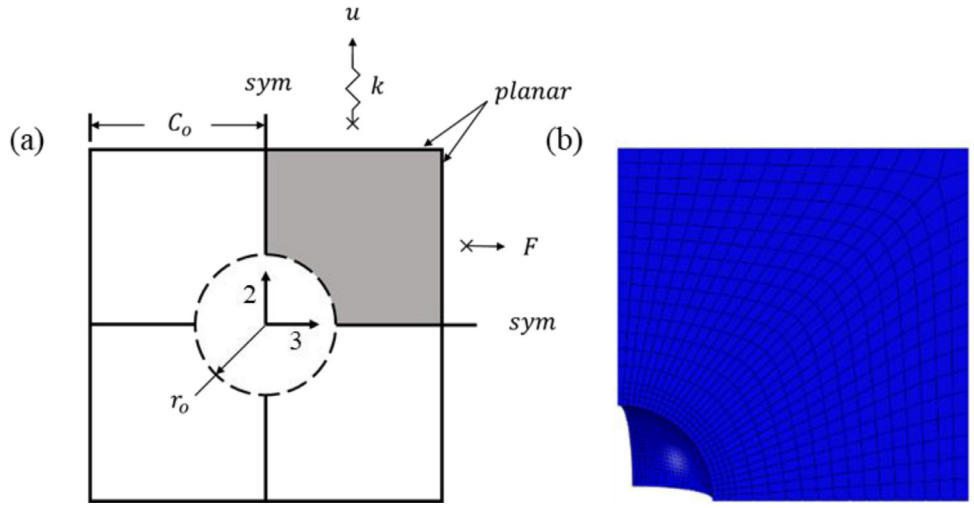

Fig. 2. (a) Two-dimensional projection of the three-dimensional cubic cell model used in this study. (b) 3D finite-element mesh of one-eighth of the unit cell corresponding to an initial void volume fraction $f_0 = 0.0104$.

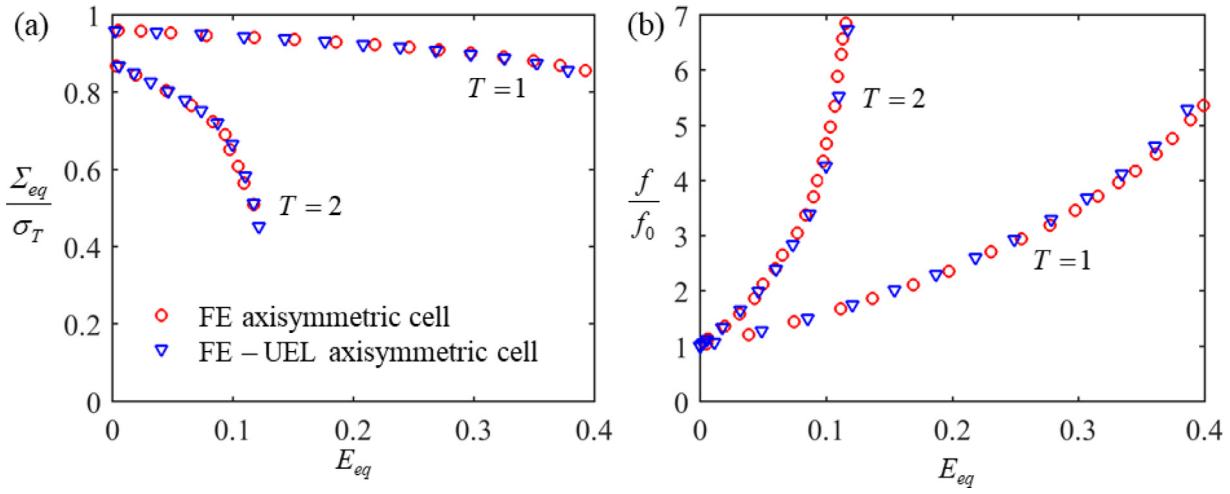

Fig. 3. Comparison between simulations for a cylindrical unit cell with plastic behavior governed by von Mises criterion and boundary conditions imposed with the developed UEL (FE-UEL axisymmetric cell) and the results reported by Koplik and Needleman (1988) (FE axisymmetric cell) for the same geometry, matrix behavior, and initial porosity $f_0 = 0.0104$. (a) Equivalent stress and equivalent plastic strain evolution for triaxiality and $T = 2$. (b) Normalized void volume fraction vs. von Mises equivalent plastic strain for triaxiality and $T = 2$.

ABAQUS user element subroutine (UEL) was developed. The UEL consists of three reference nodes which are tied to the displacement of each of the three cell faces (see Fig. 2). The detailed description of the procedure used for imposing the boundary conditions is given in the Appendix (see also Fig. A1). Since all loadings on the cell are applied inside the UEL, excellent convergence is achieved, and parallel computing can be natively used in ABAQUS. The macroscopic stresses Σ_1, Σ_2, Σ_3, are defined by forces applied at each reference node and by the areas of each face as: $\Sigma_i = F_i/A_i$. As in most unit-cell studies (e.g., Srivastava et al., 2017b) the void is considered to be traction-free. The case of the voids under internal pressure is also of technological importance (e.g., Vincent et al., 2009) and will be considered in future works.

Defining the current cell dimensions as $C_i = C_0 + U_i$, $i = 1, \ldots, 3$, the macroscopic principal plastic strains E_i^p and the macroscopic equivalent plastic strain E_{eq} are:

$$E_i^p \approx E_i = \ln\left(\frac{C_i}{C_0}\right), \; E_{eq} = \sqrt{\frac{2}{3}E_i^p E_i^p}, \tag{29}$$

wherein any elastic strain is negligible ($<10^{-5}$). The total plastic work is calculated as:

$$W^p = \sum_n (E^p_{eq,n} - E^p_{eq,n-1})\Sigma_{eq,n} \tag{30}$$

where n enumerates strain increments and Σ_{eq} is the von Mises equivalent stress.

The yield/gauge surface was calculated by interpolating the hydrostatic and equivalent stresses to a desired level of plastic work and the reference value of plastic work was selected to correspond to an equivalent plastic strain of 0.2% imposed on the fully dense material cell.

The void volume fraction of the cell is calculated as

$$f = 1 - \frac{V_0}{V}(1 - f_0), \tag{31}$$

where $V_0 = C_0^3$ is the initial volume of the unit cell, $V = C_1C_2C_3$ is the current volume of the cell, and f_0 is the initial void volume fraction (see Eq. (24)).

First, we compare the results obtained with our newly developed UEL routine for imposing boundary conditions with unit cell model results reported in the literature by Koplik and Needleman (1988) for a von Mises matrix. Given that these authors used a cylindrical unit cell with one void at the center, we use the same unit cell geometry, matrix

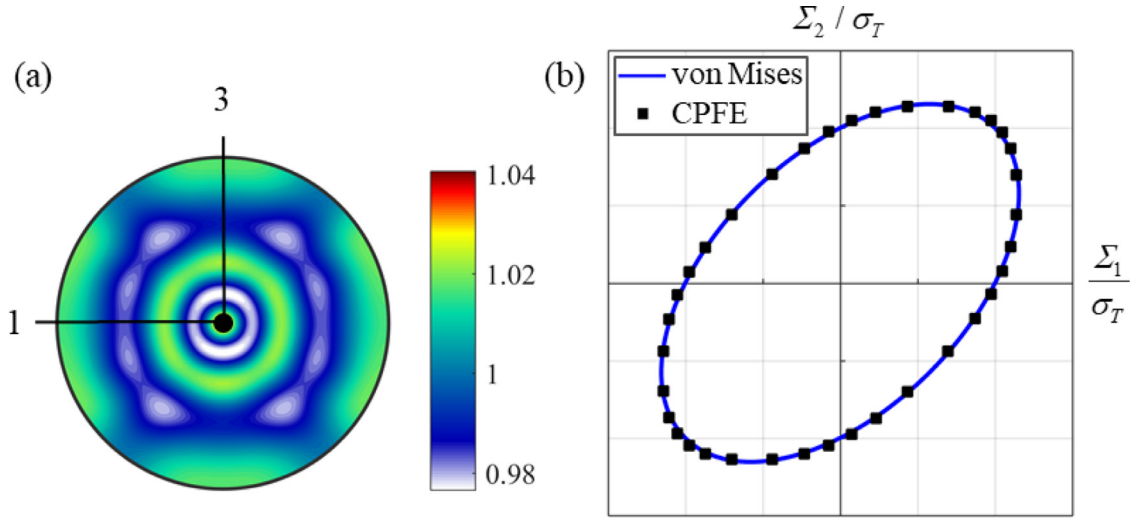

Fig. 4. (a) {111} Pole figure showing the random initial texture of the fully-dense material in the sample frame. (b) The plane stress yield surface for the fully-dense ($f = 0$) BCC polycrystal with constituent grains governed by Schmid law and calculated using CPFE in comparison with the von Mises yield surface.

behavior, initial porosity, and loading history. In Fig. 3a and b we compare the equivalent stress vs. equivalent strain response, and the void volume fraction evolution obtained for axisymmetric loadings at fixed triaxiality $T = 1$ and $T = 2$ obtained with our procedure for imposing the boundary conditions with the results reported by Koplik and Needleman (1988). The results are in excellent agreement, which validates our procedure. Note that only the results presented in Fig. 3a and b are obtained with axisymmetric (cylindrical unit cell). All the other simulations presented in this paper are done using the cubic unit cell geometry of Fig. 2.

4. Comparison between CPFE unit cell predictions and analytic criteria predictions for porous solids

The CPFE unit cell calculations were done for randomly oriented BCC polycrystals with initial texture presented in Fig. 4a and the constituent grains deforming plastically according to the rate-sensitive form of Schmid law and Non-Schmid law, respectively (see Eqs. (19) and (20)). The material texture was generated by binning the Euler orientation space. To ensure isotropy, orientations from the resulting textures were shuffled before distribution in the FE model (for more details, see Savage et al. (2017b)).

First, the CPFE yield points of a fully-dense ($f = 0$) polycrystal were calculated. The dependence of the calculated yield stresses on orientation shuffling was investigated and was less than 0.1%. Therefore, it was concluded that the behavior is isotropic. The CPFE calculated yield points corresponding to biaxial loadings ($\Sigma_3 = 0$) are shown in Fig. 4b in comparison with the yield surface according to the von Mises yield criterion. It can be seen that the numerical yield surface is isotropic (symmetry with the first bisector) and it is well approximated by the Von Mises yield criterion.

One of the objectives of the paper was to verify the features of the dilatational response of a porous Mises material (centrosymmetry; specific coupling of the invariants) put into evidence by the (Cazacu et al., 2013) criterion. This criterion was constructed using limit-analysis and the assumption of rigid-ideal plastic behavior of the void-free material. Therefore, special care was taken such that it is ensured that the polycrystal behavior is ideal perfectly plastic and that the elastic strains are negligible. Thus, in the CPFE unit cell calculations for both the fully-dense ($f = 0$) and voided polycrystals ($f \neq 0$), the elastic constants of Nb at 300 K (Carroll, 1965) were raised by one order of magnitude and the initial CRSS value lowered to tractable limits (10 MPa for each slip system), resulting in a maximum elastic strain of $E_{e,\max} \approx 2.3 \times 10^{-5}$. The value of the rate-sensitivity parameter $n = 50$ in the hardening law of the single-crystal (see Eq. (22)) was chosen (see Savage et al. (2017b)) for a detailed study on the effect of the rate-sensitivity parameter n on the overall polycrystal behavior). Comparison between the response of the matrix obtained with the CPFE code and that obtained with a rigid-ideal plastic model obeying von Mises yield criterion is shown in Fig. 5. Although CPFE predicts a gradual elasto-plastic transition for the fully-dense polycrystal, at larger strains the behavior is ideal plastic, and it is well approximated by von Mises yield criterion.

4.1. CPFE calculations obtained for the BCC porous polycrystal with slip obeying Schmid law and comparison with the analytical predictions according to Cazacu et al. (2013) criterion

The CPFE calculations for voided polycrystals were performed using the unit cell presented in Fig. 2 for axisymmetric tensile and compressive loadings corresponding to $J_3^{\Sigma} \geq 0$ (i.e., loadings such that $\Sigma_2 \geq \Sigma_1 = \Sigma_3$) and $J_3^{\Sigma} \leq 0$ ($\Sigma_2 \leq \Sigma_1 = \Sigma_3$), respectively. As mentioned, the simulations are conducted at fixed triaxialities T. For each polycrystalline material investigated simulations were conducted for various triaxialities T, ranging from $T = \pm 1/3$ (uniaxial tension and uniaxial compression, respectively) to high triaxialities ($T = \pm 10$).

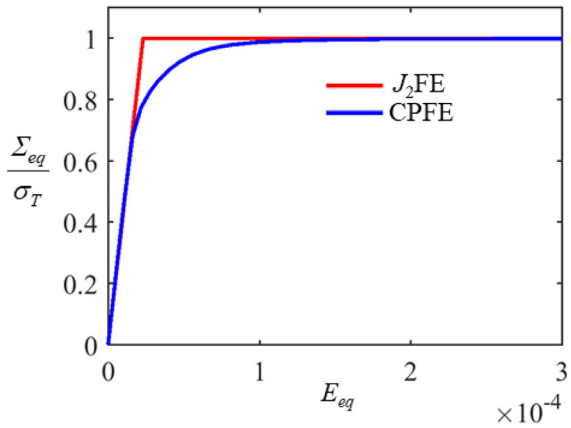

Fig. 5. Comparison of the stress-strain response in uniaxial tension of the fully dense material ($f = 0$) with rigid-ideal plastic behavior governed by von Mises yield criterion (J_2FE), and that of an isotropic BCC polycrystal with grains obeying Schmid law (CPFE).

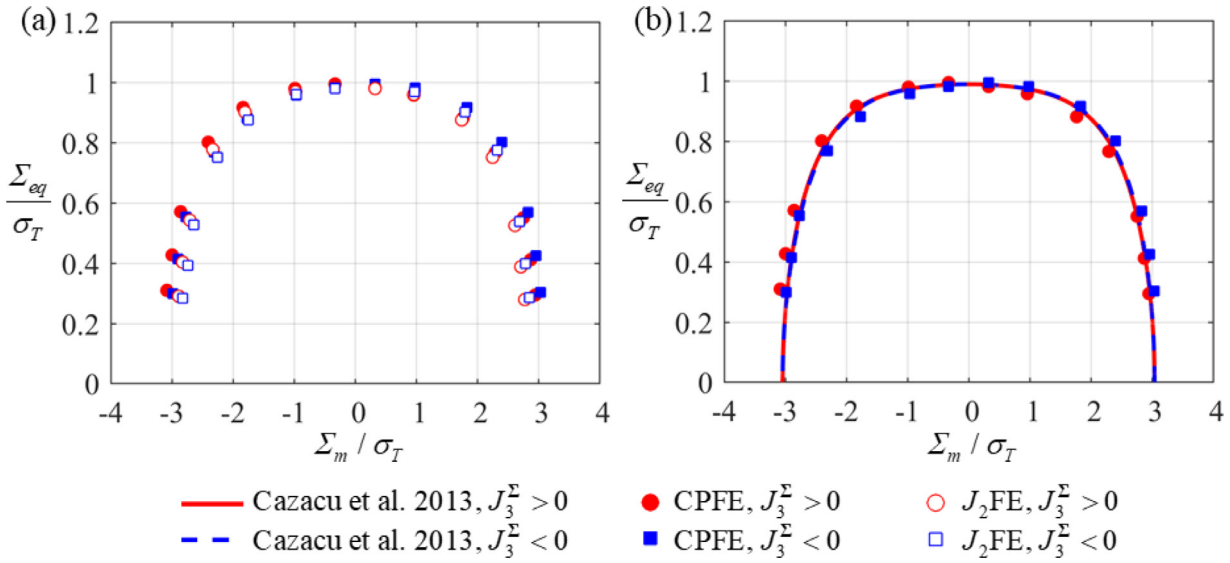

Fig. 6. Combined effects of the third-invariant and sign of the mean stress on yielding of a randomly textured porous BCC polycrystal: (a) FE unit cell numerical calculations obtained for the von Mises yield criterion (J_2FE) and the CPFE model describing the behavior of the matrix, respectively; (b) Comparison between the numerical yield points obtained with the unit cell CPFE and the predictions of the analytical model of Cazacu et al. (2013) for a porous von Mises material. Volume fraction of porosity was $f_0 = 0.0104$.

The CPFE yield points were compared to those obtained using a von Mises FE unit cell (J_2FE) with the same loading set-up, unit cell geometry, rigid ideal plastic matrix behavior (see Fig. 6a). Note that the unit cell calculations results for the porous polycrystal obtained with the crystal plasticity model for the matrix and those obtained using the classical von Mises yield criterion are almost identical.

The numerical CPFE yield points were also superposed on the projection of the yield surface for a porous von Mises material calculated with Cazacu et al., 2013) criterion (see Eqs. (3)–((8)). These results are shown in Fig. 6b. It is clearly seen that the centrosymmetry of the yield surface predicted by the (Cazacu et al., 2013a) model is confirmed. Namely, there are only two types of loadings for which the sign of J_3^Σ has no effect on the yielding of the porous material: purely deviatoric ($T = 0$) and purely hydrostatic (T very high, i.e., close to hydrostatic loadings). For all other loadings, yielding depends on J_3^Σ. Under tensile loading ($\Sigma_m = (2\Sigma_1 + \Sigma_2)/3 \geq 0$) the response for loadings such that $J_3^\Sigma \geq 0$ is softer than that for loadings corresponding to $J_3^\Sigma \leq 0$ (i.e., the curve corresponding to $J_3^\Sigma \geq 0$ is below that corresponding to $J_3^\Sigma \leq 0$) while under compressive loadings ($\Sigma_m \leq 0$) the opposite occurs. Furthermore, the yield point corresponding to a given stress-triaxiality T and $J_3^\Sigma > 0$ is symmetric, with respect to the vertical axis, $\Sigma_m = 0$, to the point corresponding to $(-T)$ and $(J_3^\Sigma \leq 0)$. Therefore, the trends in the description of yielding of porous isotropic BCC materials obeying Schmid law are predicted by the analytical model at a fraction of the computational cost of either CPFE or FE von Mises unit cell model.

Another objective of the present work is the investigation of the effects of the coupling between the mean stress and third-invariant J_3^Σ on void growth or collapse. According to Cazacu et al. (2013) model (see Eqs. (3)–(8)), void growth is faster for loadings corresponding to $J_3^\Sigma \geq 0$ than for those corresponding to$J_3^\Sigma \leq 0$. However, void collapse occurs faster for loadings where $J_3^\Sigma \leq 0$ than for those characterized by $J_3^\Sigma \geq 0$ (see also Fig. 7- lines). The void growth/collapse curves obtained with CPFE unit cell calculations and J_2-unit cell calculations for the same loadings ($T = 2$ void growth; $T = -2$ void collapse; and either $J_3^\Sigma \geq 0$ or $J_3^\Sigma \leq 0$) are also shown in Fig. 7 (symbols). The CPFE and J_2-unit cell numerical predictions also indicate that the rate of void growth/collapse depends on the sign of J_3^Σ.

To get a better insight into the combined effects of the signs of the third-invariant and mean stress on void evolution in the porous polycrystal, we further compare the local mean stress corresponding to the same level of macroscopic true strain $E_e = 0.15$ for loadings at $T = 1$ and $T = -1$ and either $J_3^\Sigma \leq 0$ or $J_3^\Sigma \geq 0$. Examination of the isocontours of the hydrostatic pressure (negative of mean stress) obtained using the CPFE unit cell approach for loadings corresponding to the same positive triaxiality ($T = 1$) show that for macroscopic loadings at $J_3^\Sigma < 0$ the distribution is completely different than in the case when the macroscopic loading is such that $J_3^\Sigma > 0$ (see Fig. 8a and c). This confirms that for the same triaxiality there is an effect of the third-invariant on the porosity evolution of the porous solid. On the other hand, the local distribution of pressure in the unit cell obtained for macroscopic loadings at $J_3^\Sigma > 0$ and $T = -1$ is almost identical with the distribution of hydrostatic pressure corresponding to macroscopic loadings at $J_3^\Sigma < 0$ and $T = 1$ (compare Fig. 8a, d, b, and c, respectively: almost identical distribution but opposite in sign). This confirms that the overall behavior of the porous Mises material for a given stress-triaxiality (T) and $J_3^\Sigma > 0$ should be the same for stress states corresponding to ($-T$) and ($J_3^\Sigma < 0$).

4.2. Comparison between analytical predictions according to Cazacu and Stewart (2009) criterion and the calculations using CPFE obtained for the BCC porous polycrystal with slip obeying Schmid law and non-Schmid law

Cazacu and Stewart (2009) have theoretically shown that SD effects in the matrix affect every aspect of the dilatational behavior of isotropic porous materials. Lebensohn and Cazacu (2012) confirmed these findings for the case when SD effects in the matrix are promoted artificially using deformation twinning only carried deformation. In this study, we examine porous BCC polycrystals for which SD effects in the polycrystalline matrix are obtained physically due to deviations from the Schmid law in the plastic flow of the constituent grains. For a direct comparison between the predictions of the (Cazacu and Stewart, 2009) model and unit cell CPFE calculations for a porous polycrystal, we need first to identify the parameter, k, involved in the (Cazacu and Stewart, 2009) model (see Eq. (9)). As mentioned, this parameter characterizes the SD effects of the matrix (fully-dense material), and it is expressible solely in terms of the ratio between the yield stress in uniaxial tension, σ_T, and the yield stress in uniaxial compression, σ_C, of the matrix:

$$k = \frac{1-h}{1+h}, \quad \text{with} \quad h = \sqrt{\frac{2-\left(\frac{\sigma_T}{\sigma_C}\right)^2}{2\left(\frac{\sigma_T}{\sigma_C}\right)^2 - 1}} \tag{32}$$

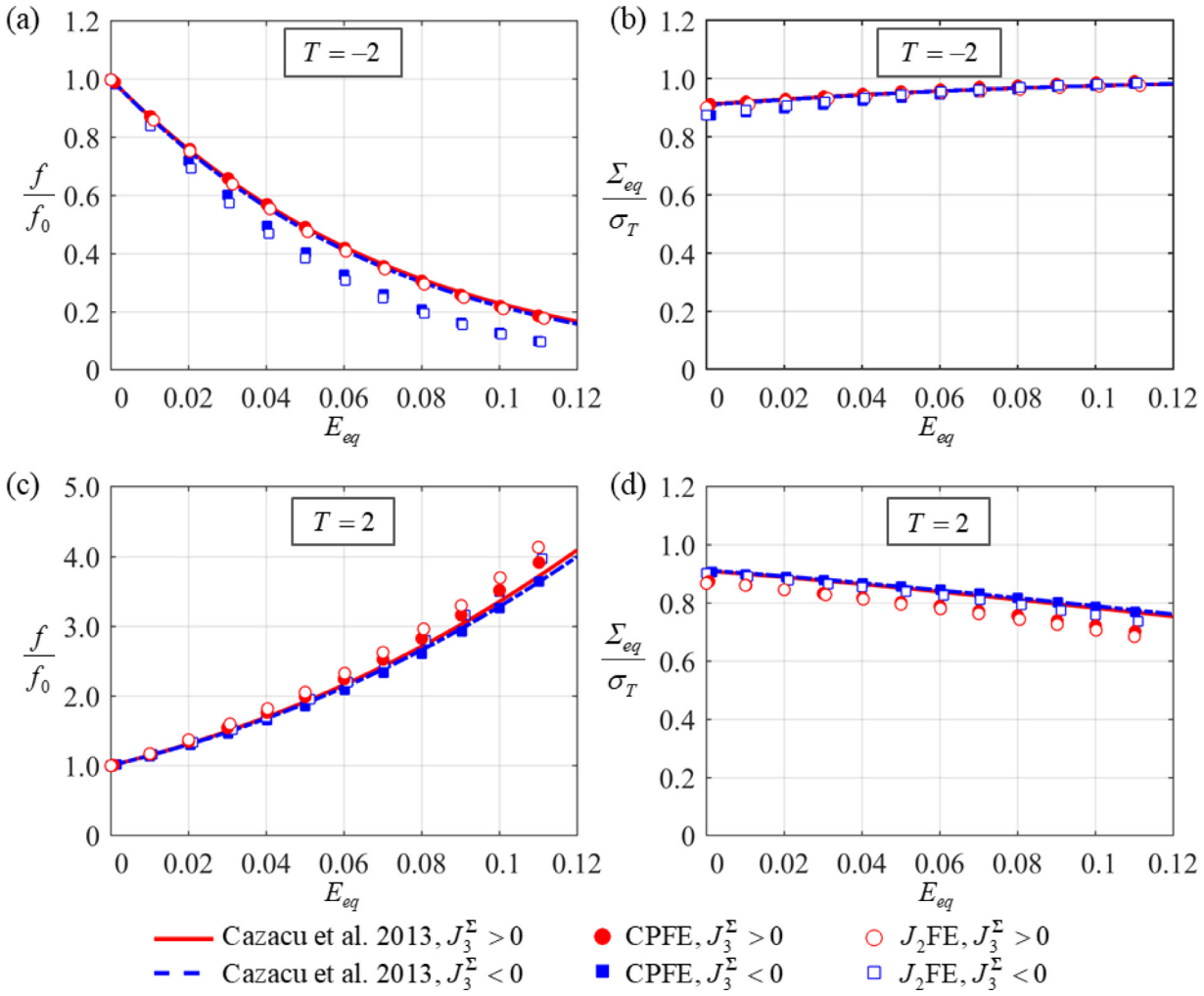

Fig. 7. Comparisons of void volume fraction and equivalent stress evolution with equivalent plastic strain predicted numerically by CPFE, J_2 FE, and analytically using Cazacu et al. (2013). Comparisons correspond to axisymmetric loadings with stress triaxiality of (a and c) $T = 2$ (Growth) and (b and d) $T = -2$ (Collapse) corresponding to either $J_3^{\Sigma} \leq 0$ or $J_3^{\Sigma} \geq 0$. The initial void volume fraction was $f_0 = 0.0104$.

To determine these yield stresses of the fully-dense polycrystal, crystal plasticity calculations were performed for the case of fully-dense ($f = 0$) isotropic BCC polycrystals with constituent grains obeying non-Schmid law given by Eqs. (19) and (20). Simulations were carried out for an untextured fully-dense BCC polycrystal considering $c_3 = -0.13$, $c_1 = c_2 = c_4 = 0$ in the non-Schmid law. The CPFE model gives a ratio $\sigma_T/\sigma_C = 1.1$ for the polycrystal, which corresponds to $k = 0.175$ (see Eq. (32)).

Fig. 9a shows the yield locus predicted by the isotropic form of the criterion (Cazacu et al., 2006) (Eq. (11)) for $k = 0.175$, in comparison with points of the gauge surface (symbols) corresponding to biaxial loadings ($\Sigma_3 = 0$) predicted by crystal plasticity with non-Schmid effects. Clearly, the isotropic form of the (Cazacu et al., 2006) yield criterion describes the plastic behavior of the fully-dense BCC polycrystal with uniform texture and SD effects. Although only two CPFE data points (the yield stress in uniaxial tension σ_T, and the yield stress in uniaxial compression, σ_C) were used for the identification and plotting of (Cazacu et al., 2006) yield locus, the agreement is excellent for all stress states.

Considering now the case of a voided untextured BCC polycrystal of the type described above, Fig. 9b shows points belonging to the gauge surfaces, corresponding to $f = 0.0104$ and stress-triaxialities ranging from $T = \pm 1/3$ (uniaxial tension and uniaxial compression, respectively) to high triaxialities ($T = \pm 10$) obtained by means of the CPFE based approach, together with the analytical yield loci according to (Cazacu and Stewart 2009) in the plane ($\Sigma_m/\sigma_T, \Sigma_e/\sigma_T$) for axisymmetric loadings corresponding to either $J_3^{\Sigma} \geq 0$ or $J_3^{\Sigma} \leq 0$. The main observation from Fig. 9b is that the strong effect of the third-invariant of the stress deviator on all stress states response predicted by (Cazacu and Stewart, 2009) criterion is indeed confirmed by the CPFE results. For the porous BCC polycrystal, whose matrix is softer in compression than in tension ($\sigma_T/\sigma_C = 1.1$), both (Cazacu and Stewart, 2009) criterion and the CPFE predictions show that the response is softer for $J_3^{\Sigma} \leq 0$ than for $J_3^{\Sigma} \geq 0$ with the maximum split corresponding to purely deviatoric loadings ($\Sigma_m = 0$). Also, it is worth noting that Cazacu and Stewart (2009) predicts for this porous material that the compressive hydrostatic yield stress is larger than the tensile hydrostatic yield stress (see Eq. (9) and Fig. 9b). The CPFE results also show that this material exhibits SD effects even for very high triaxialities.

In the case of a fully-dense isotropic BCC polycrystal with non-Schmid effects corresponding to $c_3 = 0.13$ and all other c_i values zero, the ratio between the yield stresses in uniaxial tension and uniaxial compression is $\sigma_T/\sigma_C = 0.909$. Note that such a slight tension–compression asymmetry ratio may occur in certain steel alloys (e.g., Spitzig et al., 1975). For this material using Eq. (32)), we obtain the SD parameter $k = -0.175$. Fig. 10a shows the yield surface according to the isotropic form of (Cazacu et al., 2006) criterion with $k = -0.175$ and the yield points obtained with the CPFE model with non-Schmid effects. The agreement is excellent for all stress states.

Considering next the case of the voided untextured polycrystal of

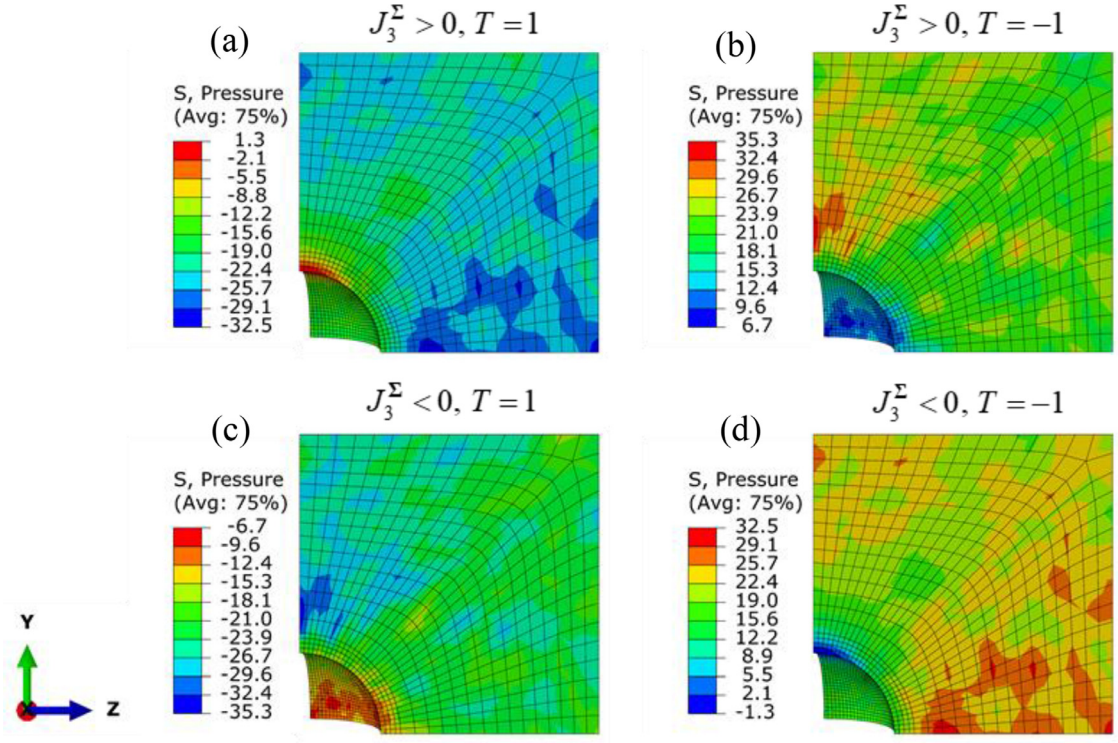

Fig. 8. Isocontours showing the local distribution hydrostatic pressure (negative of the mean stress) in the unit-cell for the applied macroscopic loadings. The amount of plastic work and the void volume fraction correspond to points on the gauge surfaces shown in Fig. 6. It is clear from these contours that the symmetry of gauge surface is preserved in CPFE unit-cell calculations (e.g., the local pressure distributions of loading $J_3^\Sigma > 0$, $T = 1$ is the same but opposite in sign to the local pressure distributions of loading $J_3^\Sigma < 0$, $T = -1$).

the same type, in Fig. 10b are shown points belonging to the gauge surfaces, corresponding to $f = 0.0104$ and stress-triaxialities ranging from $T = \pm 1/3$ (uniaxial tension and uniaxial compression, respectively) to high triaxialities ($T = \pm 10$) obtained by means of the CPFE based approach, together with the analytical yield loci according to Cazacu and Stewart, (2009), in the plane (Σ_m/σ_T,Σ_e/σ_T) for

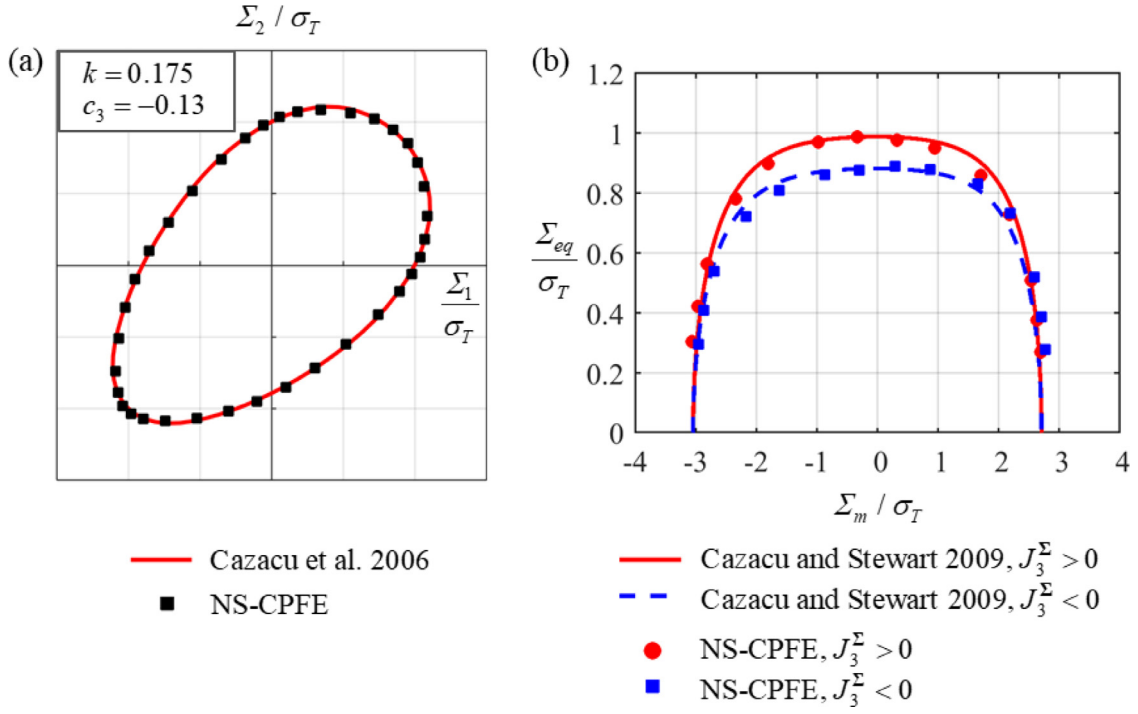

Fig. 9. (a) Yield surface for the fully-dense ($f = 0$) isotropic BCC polycrystals with $\sigma_T/\sigma_C = 1.1$ (yield stress in tension larger than in compression according to the yield criterion (Cazacu et al., 2006) ($k = 0.175$), and CPFE yield points obtained by considering non-Schmid effects (NS-CPFE) ($c_3 = -0.13$). (b) Yield surfaces of the voided ($f = 0.0104$) isotropic BCC polycrystal for axisymmetric loadings corresponding to either $J_3 > 0$ and $J_3 < 0$, respectively according to Cazacu and Stewart (2009) analytic crtierion and the yield points obtained with CPFE unit-cell calculations.

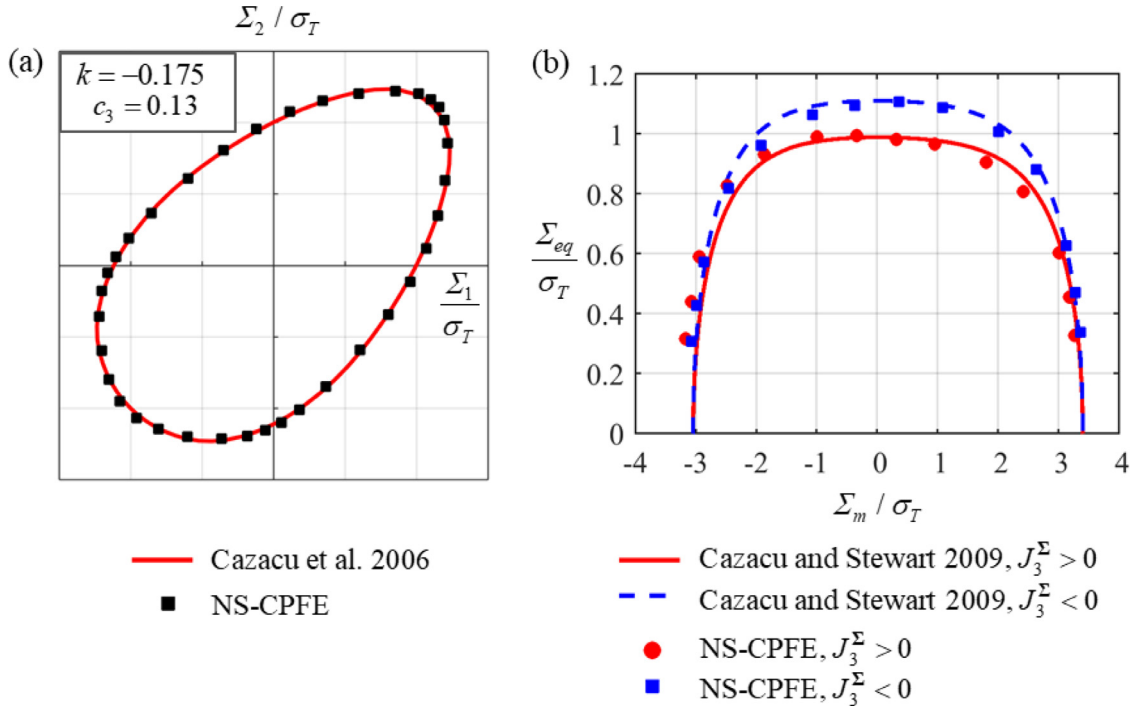

Fig. 10. (a) Yield surface for the fully-dense ($f = 0$) isotropic BCC polycrystals with $\sigma_T/\sigma_C = 0.909$ (yield stress in compression larger than in tension according to the yield criterion (Cazacu et al., 2006) ($k = -0.175$), and CPFE yield points obtained by considering non-Schmid effects (NS-CPFE) ($c_3 = 0.13$). (b) Yield surfaces of the voided ($f = 0.0104$) isotropic BCC polycrystal for axisymmetric loadings corresponding to either $J_3 > 0$ and $J_3 < 0$, respectively according to (Cazacu and Stewart, 2009) analytic crtierion and the yield points obtained with CPFE unit-cell calculations.

axisymmetric loadings corresponding to either $J_3^{\Sigma} \geq 0$ or $J_3^{\Sigma} \leq 0$. It is very interesting to note that for this material whose matrix is softer in tension than in compression, for any given triaxiality T, the response of the voided material is softer for loadings at $J_3^{\Sigma} \geq 0$ than for loadings at $J_3^{\Sigma} \leq 0$. For purely deviatoric loading ($T = 0$), the effect of the third invariant is the strongest while for triaxialities approaching infinity, the effect of J_3^{Σ} starts to decrease, and the yield surfaces for $J_3^{\Sigma} \geq 0$ and for $J_3^{\Sigma} \leq 0$ coincide. In contrast to the case when the matrix has no SD effects (governed by von Mises; see Fig. 6), the voided polycrystal displays SD effects irrespective of the triaxiality. In particular, for hydrostatic loadings (triaxiality infinite), the absolute value of the yield pressure corresponding to compressive hydrostatic loading is slightly lower than the mean stress corresponding to tensile hydrostatic loading.

5. Conclusions

In this paper, we used the unit cell modeling approach in conjunction with crystal plasticity finite element (CPFE) model to study the dilatational response of porous polycrystals and verify the specific effects of the plastic deformation of the matrix on yielding and void evolution that were suggested in recent analytic criteria. The unit cell modeling approach in conjunction with CPFE was used to generate gauge surfaces for porous untextured BCC polycrystals deforming by slip at single crystal level. Both Schmid and non-Schmid activation criteria for plastic deformation were considered. The simulations were conducted for axisymmetric tensile and compressive loadings corresponding to a fixed value of the stress triaxiality. The main observations are the following:

(1) In the case when slip is governed by the classic Schmid law and there is no preferred texture, the fully-dense polycrystal's plastic behavior is well described by von Mises yield criterion. For a porous polycrystal of the same type, the main features predicted by the (Cazacu et al., 2013) criterion are confirmed, namely:
   (a) the yield surface of the porous material is centrosymmetric;
   (b) there is a specific coupling between the signs of the mean stress and third-invariant of the stress-deviator on yielding and void growth/collapse;
   (c) there is no effect of the third-invariant of the stress deviator for purely deviatoric loadings;
   (d) there are no strength differential (SD) effects for hydrostatic loadings.

(2) In the case when slip deviates from Schmid law and there is no preferred orientation, the SD effects on the yielding behavior of the fully-dense isotropic polycrystal can be described by (Cazacu et al., 2006) yield criterion. Furthermore, for a voided polycrystal of the same type, as described by (Cazacu and Stewart, 2009) analytic criterion, the sensitivity of the mechanical response to the third-invariant of the stress deviator correlates with the matrix tension–compression asymmetry ratio. Specifically,
   (a) If deviations from Schmid law induce an SD ratio of the fully-dense polycrystal such that $\sigma_C/\sigma_T > 1$:
      i) both the analytical yield surface and the CPFE yield locus corresponding to stress states for which $J_3^{\Sigma} \leq 0$ is above that corresponding to $J_3^{\Sigma} \geq 0$;
      ii) the strongest effect of J_3^{Σ} is for purely deviatoric loadings;
      iii) the porous material displays SD effects irrespective of the triaxiality. In particular, for hydrostatic loadings (triaxiality infinite), the absolute value of the yield pressure corresponding to compressive hydrostatic loading is slightly larger than the mean stress corresponding to tensile hydrostatic loading.
   (b) If deviations from Schmid law induce an SD ratio of the fully-dense polycrystal characterized by an SD ratio $\sigma_C/\sigma_T < 1$:
      i) both the analytical yield surface and the CPFE yield locus corresponding to stress states for which $J_3^{\Sigma} \geq 0$ is above that corresponding to $J_3^{\Sigma} \leq 0$;
      ii) the strongest effect of J_3^{Σ} is for purely deviatoric loadings;
      iii) the porous material displays SD effects irrespective of the triaxiality. In particular, for hydrostatic loadings (triaxiality

infinite), the absolute value of the yield pressure corresponding to compressive hydrostatic loading is slightly lower than the mean stress corresponding to tensile hydrostatic loading.

In closing we would like to point out that although the agreement obtained between the numerical CPFE predictions and the analytical results is not necessarily quantitative (due to different assumptions involved in both approximations to the problem of dilatational plasticity, the strain rate sensitivity, and homogenization), the good qualitative agreement serves as cross-validation of both approaches. Most importantly, it was shown that micromechanically motivated macroscopic models can predict with accuracy the influence of the stress history on yielding and void evolution in isotropic porous polycrystalline materials. It is also to be noted that these analytic macroscopic models can be efficiently implemented as a material subroutine in FE codes for engineering applications involving polycrystalline materials with complex dilatational plastic behavior; and that their respective material parameters can be identified from CPFE simulations. These aspects will be studied in future works.

Acknowledgments

Marko Knezevic acknowledges support for this research from the US Army Research Laboratory under cooperative agreement No. W911NF-15-2-0084 and the US National Science Foundation (NSF) under grant No. CMMI-1650641. Daniel J. Savage acknowledges support through the NSF graduate research fellowship program. Oana Cazacu and Nitin Chandola acknowledge partial support provided for this work from the Army Research Office (ARO) under grant W911NF-16-1-0159, and fruitful discussions and insights provided by Dr. Ralph Anthenien.

Supplementary materials

Supplementary material associated with this article can be found, in the online version, at doi:10.1016/j.mechmat.2018.08.004.

Appendix A

In the following, we describe the procedure used for imposing constant stress triaxiality on the unit cell during the entire loading history.

Fig. A1 shows the boundary conditions and the ABAQUS user element subroutine (UEL) used for conducting the simulations. The coordinate system used is defined with respect to the center of the void. To simulate one-eighth of the unit cell, symmetry boundary conditions are applied on the interior of the cell, i.e. for symmetry planes 1, 2, and 3:

$$u_1(0, x_2, x_3) = ur_2(0, x_2, x_3) = ur_3(0, x_2, x_3) = 0 \tag{A1}$$

$$u_2(x_1, 0, x_3) = ur_1(x_1, 0, x_3) = ur_3(x_1, 0, x_3) = 0 \tag{A2}$$

$$u_3(x_1, x_2, 0) = ur_1(x_1, x_2, 0) = ur_2(x_1, x_2, 0) = 0 \tag{A3}$$

where the variables, u and ur are the translational and angular displacements respectively. The subscript $i = 1, \ldots, 3$ denotes the respective Cartesian coordinate axis i.e. 1, 2, or 3.

The translational displacements U_i of the cube faces are tied to the displacements of a reference node M (i.e. $U_i = u_i^M$), located at the intersection of the three planes, using multipoint constraints (MPCs). This constraint ensures the periodicity of the cell. The current cell dimensions are defined with respect to the node M as,

$$C_i = C_0 + u_i^M \tag{A4}$$

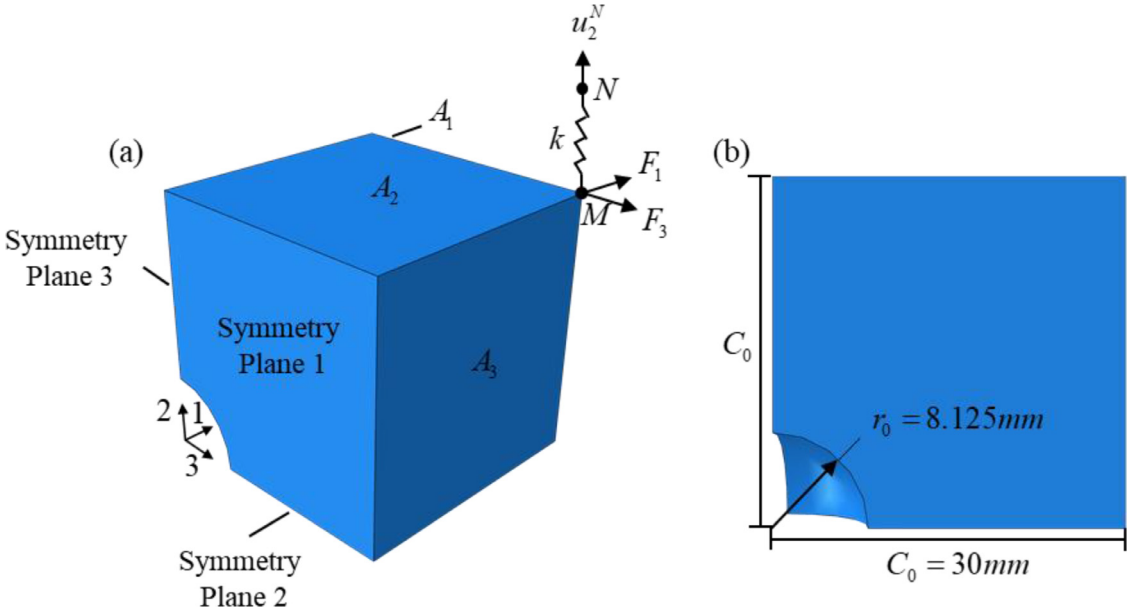

Fig. A1. (a) Cell definition and UEL nomenclature. (b) Dimensions of the unit cell corresponding to an initial void volume fraction of $f_0 = 0.0104$.

where C_0 is the initial length of the cubic cell (Fig. A1b). The areas of the faces of the deformed cubic cell are then given as,

$$A_1 = C_2C_3,\ A_2 = C_1C_3,\ \text{and}\ A_3 = C_1C_2 \tag{A5}$$

The stress boundary conditions are applied through a single reference node, *M*, in the UEL subroutine. The user element (UEL) is defined as a linear elastic spring between a free node *N* (see Fig. A1a) and the edge node *M*. For a given displacement u_2^N, a known force is applied to *M* and thus to A_2 by either stretching or compressing the spring. Appropriate forces are calculated and applied simultaneously on the faces A_1 and A_3 to ensure the required value of the stress triaxiality T^{Σ}. Note that, the overall Cauchy stress on each face is defined as:

$$\Sigma_i = \frac{F_i^M}{A_i}. \tag{A6}$$

The trial displacement at *M* and the prescribed displacement at *N* are made available in the UEL as part of the standard solution procedure in ABAQUS. The force on node *M* due to the relative displacement between nodes *M* and *N* is:

$$F_2^M = (u_2^N - u_2^M)k \tag{A7}$$

where a suitable stiffness *k* is approximately 10–100 times larger than the Young's modulus (Ha and Kim, 2010) of the matrix material of the unit cell.

Given that we consider only axisymmetric loadings, the other two forces applied on node *M* are then calculated as,

$$F_1^M = \frac{A_1H}{A_2}F_2^M \text{and} F_3^M = \frac{A_3H}{A_2}F_2^M \tag{A8}$$

where, F_1^M and F_3^M are forces applied on face 1 and 3, respectively, H is the stress ratio between the two independent overall Cauchy stress components.

Note that for axisymmetric loadings ($\Sigma_1 = \Sigma_3$)

$$T^{\Sigma} = \frac{2\Sigma_1 + \Sigma_2}{3|\Sigma_1 - \Sigma_2|} \tag{A9}$$

For $\Sigma_2 \neq 0$, the stress ratio $H = \Sigma_1/\Sigma_2$ on substitution in Eq. (A9) gives,

$$T^{\Sigma} = \frac{2H + 1}{3|H - 1|} \tag{A10}$$

As mentioned in Section 1:

a. For the same value of stress triaxiality T^{Σ}, axisymmetric loading can correspond to $J_3^{\Sigma} > 0$ or $J_3^{\Sigma} < 0$ during the entire deformation process.
b. Moreover, in this paper we consider both axisymmetric tensile loading with $T^{\Sigma} > 0$ and axisymmetric compressive loading with $T^{\Sigma} < 0$.

For all these loading scenarios, two cases arise,

I. For $J_3^{\Sigma} > 0$, $T^{\Sigma} > 0$ or $J_3^{\Sigma} < 0$, $T^{\Sigma} < 0$

$$H = \frac{3T^{\Sigma} - 1}{3T^{\Sigma} + 2} \tag{A11}$$

II. For $J_3^{\Sigma} > 0$, $T^{\Sigma} < 0$ or $J_3^{\Sigma} < 0$, $T^{\Sigma} > 0$

$$H = \frac{3T^{\Sigma} + 1}{3T^{\Sigma} - 2} \tag{A12}$$

For case I, using a truss element formulization as in Lin et al. (2006), the forces applied on the faces 1 and 3 (see Eq. (A8)) can be defined in a UEL stiffness matrix. Their contribution to the Jacobian and overall stiffness of the cell model is therefore accounted for and the rate of convergence is excellent. Thus, the nonsymmetric system of equations defined in the UEL is explicitly given as

$$\begin{bmatrix} 0 & \frac{A_1H}{A_2}k & 0 & 0 & -\frac{A_1H}{A_2}k & 0 \\ 0 & k & 0 & 0 & -k & 0 \\ 0 & \frac{A_3H}{A_2}k & 0 & 0 & -\frac{A_3H}{A_2}k & 0 \\ 0 & 0 & 0 & 0 & 0 & 0 \\ 0 & -k & 0 & 0 & k & 0 \\ 0 & 0 & 0 & 0 & 0 & 0 \end{bmatrix} \begin{Bmatrix} u_1^M \\ u_2^M \\ u_3^M \\ u_1^N \\ u_2^N \\ u_3^N \end{Bmatrix} = \begin{Bmatrix} F_1^M \\ F_2^M \\ F_3^M \\ 0 \\ F_2^N \\ 0 \end{Bmatrix} \tag{A13}$$

The main convergence criteria for this scheme are a suitable stiffness value, *k*, and ensuring that the direction of applied displacement u_2^N is the same as that of the planar displacement U_2. For case II (i.e., for loadings ($J_3^{\Sigma} > 0,\ T^{\Sigma} < 0$) and ($J_3^{\Sigma} < 0,\ T^{\Sigma} > 0$)) u_2^N and U_2 will have opposite directions; therefore, the spring element must be reoriented to either the 1 or the 3 direction.

References

Alleman, C., Ghosh, S., Luscher, D., Bronkhorst, C.A., 2014. Evaluating the effects of loading parameters on single-crystal slip in tantalum using molecular mechanics. Philos. Mag. 94, 92–116.

Alves, J.L., Benoit, R.-B., Oana, C., 2014. Importance of the coupling between the sign of the mean stress and the third invariant on the rate of void growth and collapse in porous solids with a von Mises matrix. Model. Simul. Mater. Sci. Eng. 22, 025005.

Anderson, T.L., 2017. Fracture Mechanics: Fundamentals and Applications, Fourth ed. CRC press, Boca Raton, FL.

Ardeljan, M., Beyerlein, I.J., Knezevic, M., 2014. A dislocation density based crystal plasticity finite element model: application to a two-phase polycrystalline HCP/BCC composites. J. Mech. Phys. Solids 66, 16–31.

Ardeljan, M., Beyerlein, I.J., Knezevic, M., 2017. Effect of dislocation density-twin interactions on twin growth in AZ31 as revealed by explicit crystal plasticity finite element modeling. Int. J. Plast. 99, 81–101.

Ardeljan, M., Beyerlein, I.J., McWilliams, B.A., Knezevic, M., 2016. Strain rate and temperature sensitive multi-level crystal plasticity model for large plastic deformation behavior: application to AZ31 magnesium alloy. Int. J. Plast. 83, 90–109.

Ardeljan, M., Knezevic, M., Nizolek, T., Beyerlein, I.J., Mara, N.A., Pollock, T.M., 2015. A study of microstructure-driven strain localizations in two-phase polycrystalline HCP/BCC composites using a multi-scale model. Int. J. Plast. 74, 35–57.

Asaro, R.J., Needleman, A., 1985. Texture development and strain hardening in rate dependent polycrystals. Acta Metall. Mater. 33, 923–953.

Barsoum, I., Faleskog, J., 2007. Rupture mechanisms in combined tension and shear – experiments. Int. J. Solids Struct. 44, 1768–1786.

Barthélémy, J.F., Dormieux, L., 2004. A micromechanical approach to the strength criterion of Drucker–Prager materials reinforced by rigid inclusions. Int. J. Numer. Anal. Methods Geomech. 28, 565–582.

Carroll, K.J., 1965. Elastic constants of Niobium from 4.2 to 300 K. J. Appl. Phys. 36, 3689–3690.

Cazacu, O., Plunkett, B., Barlat, F., 2006. Orthotropic yield criterion for hexagonal closed packed metals. Int. J. Plast. 22, 1171–1194.

Cazacu, O., Revil-Baudard, B., Lebensohn, R.A., Garajeu, M., 2013. On the combined effect of pressure and third invariant on yielding of porous solids with von Mises matrix. J. Appl. Mech. 80, 064501–064505.

Cazacu, O., Stewart, J.B., 2009. Analytic plastic potential for porous aggregates with matrix exhibiting tension–compression asymmetry. J. Mech. Phys. Solids 57, 325–341.

Dao, M., Asaro, R.J., 1993. Non-Schmid effects and localized plastic flow in intermetallic alloys. Mater. Sci. Eng. A 170, 143–160.

Dunand, M., Mohr, D., 2011. On the predictive capabilities of the shear modified Gurson and the modified Mohr–Coulomb fracture models over a wide range of stress triaxialities and Lode angles. J. Mech. Phys. Solids 59, 1374–1394.

Franciosi, P., 1983. Glide mechanisms in b.c.c. crystals: an investigation of the case of [alpha]-iron through multislip and latent hardening tests. Acta Metall. 31, 1331–1342.

Franciosi, P., 1985. The concepts of latent hardening and strain hardening in metallic single crystals. Acta Metall. 33, 1601–1612.

Ghorbanpour, S., Zecevic, M., Kumar, A., Jahedi, M., Bicknell, J., Jorgensen, L., Beyerlein, I.J., Knezevic, M., 2017. A crystal plasticity model incorporating the effects of precipitates in superalloys: application to tensile, compressive, and cyclic deformation of Inconel 718. Int. J. Plast. 99, 162–185.

Gilles, G., Hammami, W., Libertiaux, V., Cazacu, O., Yoon, J., Kuwabara, T., Habraken, A., Duchêne, L., 2011. Experimental characterization and elasto-plastic modeling of the quasi-static mechanical response of TA-6V at room temperature. Int. J. Solids Struct. 48, 1277–1289.

Gröger, R., Racherla, V., Bassani, J., Vitek, V., 2008. Multiscale modeling of plastic deformation of molybdenum and tungsten: II. Yield criterion for single crystals based on atomistic studies of glide of 1/2<111>screw dislocations. Acta Materialia 56, 5412–5425.

Guo, T., Faleskog, J., Shih, C., 2008. Continuum modeling of a porous solid with pressure-sensitive dilatant matrix. J. Mech. Phys. Solids 56, 2188–2212.

Gurson, A.L., 1977. Continuum theory of ductile rupture by void nucleation and growth: part I – yield criteria and flow rules for porous ductile media. J. Eng. Mater. Technol. 99, 2–15.

Ha, S., Kim, K., 2010. Void growth and coalescence in f.c.c. single crystals. Int. J. Mech. Sci. 52, 863–873.

Hill, R., 1967. The essential structure of constitutive laws for metal composites and polycrystals. J. Mech. Phys. Solids 15, 79–95.

Hosford, W.F., Allen, T.J., 1973. Twinning and directional slip as a cause for a strength differential effect. Metall. Trans. 4, 1424–1425.

Hosford, W.F., Caddell, R.M., 1993. Metal Forming Mechanics and Metallurgy. Prentice-Hall, Inc, Englewood Cliffs, New Jersey.

Hosokawa, A., Wilkinson, D.S., Kang, J., Maire, E., 2012. Effect of triaxiality on void growth and coalescence in model materials investigated by X-ray tomography. Acta Materialia 60, 2829–2839.

Ito, K., Vitek, V., 2001. Atomistic study of non-Schmid effects in the plastic yielding of bcc metals. Philos. Mag. A 81, 1387–1407.

Kalidindi, S.R., Bronkhorst, C.A., Anand, L., 1992. Crystallographic texture evolution in bulk deformation processing of FCC metals. J. Mech. Phys. Solids 40, 537–569.

Knezevic, M., Beyerlein, I.J., Lovato, M.L., Tomé, C.N., Richards, A.W., McCabe, R.J., 2014. A strain-rate and temperature dependent constitutive model for BCC metals incorporating non-Schmid effects: application to tantalum–tungsten alloys. Int. J. Plast. 62, 93–104.

Knezevic, M., Capolungo, L., Tomé, C.N., Lebensohn, R.A., Alexander, D.J., Mihaila, B., McCabe, R.J., 2012. Anisotropic stress-strain response and microstructure evolution of textured α-uranium. Acta. Mater. 60, 702–715.

Knezevic, M., Crapps, J., Beyerlein, I.J., Coughlin, D.R., Clarke, K.D., McCabe, R.J., 2016a. Anisotropic modeling of structural components using embedded crystal plasticity constructive laws within finite elements. Int. J. Mech. Sci. 105, 227–238.

Knezevic, M., Lebensohn, R.A., Cazacu, O., Revil-Baudard, B., Proust, G., Vogel, S.C., Nixon, M.E., 2013a. Modeling bending of α-titanium with embedded polycrystal plasticity in implicit finite elements. Mater. Sci. Eng. A 564, 116–126.

Knezevic, M., Levinson, A., Harris, R., Mishra, R.K., Doherty, R.D., Kalidindi, S.R., 2010. Deformation twinning in AZ31: influence on strain hardening and texture evolution. Acta. Mater. 58, 6230–6242.

Knezevic, M., McCabe, R.J., Tomé, C.N., Lebensohn, R.A., Chen, S.R., Cady, C.M., Gray Iii, G.T., Mihaila, B., 2013b. Modeling mechanical response and texture evolution of α-uranium as a function of strain rate and temperature using polycrystal plasticity. Int. J. Plast. 43, 70–84.

Knezevic, M., Zecevic, M., Beyerlein, I.J., Bhattacharyya, A., McCabe, R.J., 2015a. Predicting texture evolution in Ta and Ta-10W alloys using polycrystal plasticity. JOM 67, 2670–2674.

Knezevic, M., Zecevic, M., Beyerlein, I.J., Bingert, J.F., McCabe, R.J., 2015b. Strain rate and temperature effects on the selection of primary and secondary slip and twinning systems in HCP Zr. Acta. Mater. 88, 55–73.

Knezevic, M., Zecevic, M., Beyerlein, I.J., Lebensohn, R.A., 2016b. A numerical procedure enabling accurate descriptions of strain rate-sensitive flow of polycrystals within crystal visco-plasticity theory. Comput. Methods Appl. Mech. Eng. 308, 468–482.

Koplik, J., Needleman, A., 1988. Void growth and coalescence in porous plastic solids. Int. J. Solids Struct. 24, 835–853.

Lebensohn, R.A., Cazacu, O., 2012. Effect of single-crystal plastic deformation mechanisms on the dilatational plastic response of porous polycrystals. Int. J. Solids Struct. 49, 3838–3852.

Lebensohn, R.A., Idiart, M.I., Castañeda, P.P., 2012. Modeling microstructural effects in dilatational plasticity of polycrystalline materials. Procedia IUTAM 3, 314–330.

Lebensohn, R.A., Montagnat, M., Mansuy, P., Duval, P., Meysonnier, J., Philip, A., 2009. Modeling viscoplastic behavior and heterogeneous intracrystalline deformation of columnar ice polycrystals. Acta Mater. 57, 1405–1415.

Lebensohn, R.A., Rollett, A.D., Suquet, P., 2011. Fast fourier transform-based modeling for the determination of micromechanical fields in polycrystals. JOM 63, 13–18.

Lim, H., Weinberger, C.R., Battaile, C.C., Buchheit, T.E., 2013. Application of generalized non-Schmid yield law to low-temperature plasticity in bcc transition metals. Model. Simul. Mater. Sci. Eng. 21, 045015.

Lin, R., Steglich, D., Brocks, W., Betten, J., 2006. Performing RVE calculations under constant stress triaxiality for monotonous and cyclic loading. Int. J. Numer. Methods Eng. 66, 1331–1360.

Lipinski, P., Berveiller, M., 1989. Elastoplasticity of micro-inhomogeneous metals at large strains. Int. J. Plast. 5, 149–172.

Lou, Y., Huh, H., 2013. Evaluation of ductile fracture criteria in a general three-dimensional stress state considering the stress triaxiality and the lode parameter. Acta Mech. Solida Sin. 26, 642–658.

Ma, A., Roters, F., Raabe, D., 2007. A dislocation density based constitutive law for BCC materials in crystal plasticity FEM. Comput. Mater. Sci. 39, 91–95.

Mandel, J., 1973. Plasticité Classique Et viscoplasticité Course held at the Department of Mechanics of Solids September–October 1971. Springer, Udine, Wien, New York.

McClintock, F.A., 1968. A criterion for ductile fracture by the growth of holes. J. Appl. Mech. 35, 363–371.

Nixon, M.E., Cazacu, O., Lebensohn, R.A., 2010. Anisotropic response of high-purity α-titanium: experimental characterization and constitutive modeling. Int. J. Plast. 26, 516–532.

Patra, A., Zhu, T., McDowell, D.L., 2014. Constitutive equations for modeling non-Schmid effects in single crystal bcc-Fe at low and ambient temperatures. Int. J. Plast. 59, 1–14.

Peeters, B., Hoferlin, E., Van Houtte, P., Aernoudt, E., 2001. Assessment of crystal plasticity based calculation of the lattice spin of polycrystalline metals for FE implementation. Int. J. Plast. 17, 819–836.

Revil-Baudard, B., Cazacu, O., Flater, P., Chandola, N., Alves, J., 2016. Unusual plastic deformation and damage features in Titanium: experimental tests and constitutive modeling. J. Mech. Phys. Solids 88, 100–122.

Savage, D.J., Beyerlein, I.J., Knezevic, M., 2017a. Coupled texture and non-Schmid effects on yield surfaces of body-centered cubic polycrystals predicted by a crystal plasticity finite element approach. Int. J. Solids Struct. 109, 22–32.

Savage, D.J., Cazacu, O., Knezevic, M., 2017b. Dilational response of voided polycrystals. JOM 69, 942–947.

Spitzig, W.A., Sober, R.J., Richmond, O., 1975. Pressure dependence of yielding and associated volume expansion in tempered martensite. Acta Metallur. 23, 885–893.

Srivastava, A., Needleman, A., 2015. Effect of crystal orientation on porosity evolution in a creeping single crystal. Mech. Mater. 90, 10–29.

Srivastava, A., Revil-Baudard, B., Cazacu, O., Needleman, A., 2017a. A model for creep of porous crystals with cubic symmetry. Int. J. Solids Struct. 110–111, 67–79.

Srivastava, A., Revil-Baudard, B., Cazacu, O., Needleman, A., 2017b. A model for creep of porous crystals with cubic symmetry. Int. J. Solids Struct. 110–111, 67–79.

Trillat, M., Pastor, J., Francescato, P., 2006. Yield criterion for porous media with spherical voids. Mech. Res. Commun. 33, 320–328.

Tvergaard, V., 1981. Influence of voids on shear band instabilities under plane strain conditions. Int. J. Fract. 17, 389–407.

Tvergaard, V., Needleman, A., 1984. Analysis of the cup-cone fracture in a round tensile bar. Acta Metallur. 32, 157–169.

Vincent, P.-G., Monerie, Y., Suquet, P., 2009. Porous materials with two populations of

voids under internal pressure: I. instantaneous constitutive relations. Int. J. Solids Struct. 46, 480–506.
Wang, Z.Q., Beyerlein, I.J., 2011. An atomistically-informed dislocation dynamics model for the plastic anisotropy and tension–compression asymmetry of BCC metals. Int. J. Plast. 27, 1471–1484.
Yerra, S.K., Tekog˘lu, C., Scheyvaerts, F., Delannay, L., Van Houtte, P., Pardoen, T., 2010. Void growth and coalescence in single crystals. Int. J. Solids Struct. 47, 1016–1029.
Zecevic, M., Beyerlein, I.J., Knezevic, M., 2017. Coupling elasto-plastic self-consistent crystal plasticity and implicit finite elements: applications to compression, cyclic tension-compression, and bending to large strains. Int. J. Plast. 93, 187–211.
Zecevic, M., Beyerlein, I.J., Knezevic, M., 2018. Activity of pyramidal I and II <c +a>slip in Mg alloys as revealed by texture development. J. Mech. Phys. Solids 111, 290–307.
Zecevic, M., Knezevic, M., Beyerlein, I.J., McCabe, R.J., 2016a. Texture formation in orthorhombic alpha-uranium under simple compression and rolling to high strains. J. Nucl. Mater. 473, 143–156.
Zecevic, M., Korkolis, Y.P., Kuwabara, T., Knezevic, M., 2016b. Dual-phase steel sheets under cyclic tension–compression to large strains: experiments and crystal plasticity modeling. J. Mech. Phys. Solids 96, 65–87.